RESEARCH ARTICLE

RF Exposure Assessment in ITS-5.9 GHz V2X Connectivity and Vehicle Wireless Technologies: A Numerical and Experimental Approach

YIZHEN YANG[1], BARBARA M. MASINI[2], (Senior Member, IEEE),
GÜNTER VERMEEREN[1], (Member, IEEE), DANIEL VAN DEN AKKER[3], SAM AERTS[4],
LEEN VERLOOCK[1], EMMA CHIARAMELLO[2], (Member, IEEE), MARTA BONATO[2],
JOE WIART[5], (Senior Member, IEEE), GABRIELLA TOGNOLA[2],
AND WOUT JOSEPH[1], (Senior Member, IEEE)

[1]Department of Information Technology, Ghent University/imec, 9052 Ghent, Belgium
[2]Institute of Electronics, Computer and Telecommunication Engineering (IEIIT), National Research Council (CNR), 20133 Milan, Italy
[3]IDLab, Department of Computer Science, University of Antwerp/imec, 2000 Antwerp, Belgium
[4]Smart Sensor Systems Research Group, Faculty of Technology, Innovation and Society, The Hague University of Applied Sciences, 2628 AL Delft, The Netherlands
[5]Department of Communication and Electronic (COMELEC), Institut Mines-Télécom, 91120 Palaiseau, France

Corresponding author: Yizhen Yang (yizhen.yang@ugent.be)

ABSTRACT As Vehicle-to-Everything (V2X) communication technologies gain prominence, ensuring human safety from radiofrequency (RF) electromagnetic fields (EMF) becomes paramount. This study critically examines human RF exposure in the context of ITS-5.9 GHz V2X connectivity, employing a combination of numerical dosimetry simulations and targeted experimental measurements. The focus extends across Road-Side Units (RSUs), On-Board Units (OBUs), and, notably, the advanced vehicular technologies within a Tesla Model S, which includes Bluetooth, Long Term Evolution (LTE) modules, and millimeter-wave (mmWave) radar systems. Key findings indicate that RF exposure levels for RSUs and OBUs, as well as from Tesla's integrated technologies, consistently remain below the International Commission on Non-Ionizing Radiation Protection (ICNIRP) exposure guidelines by a significant margin. Specifically, the maximum exposure level around RSUs was observed to be 10 times lower than ICNIRP reference level, and Tesla's mmWave radar exposure did not exceed 0.29 W/m^2, well below the threshold of 10 W/m^2 set for the general public. This comprehensive analysis not only corroborates the effectiveness of numerical dosimetry in accurately predicting RF exposure but also underscores the compliance of current V2X communication technologies with exposure guidelines, thereby facilitating the protective advancement of intelligent transportation systems against potential health risks.

INDEX TERMS Electromagnetic field exposure, connected vehicles, in-lab/situ measurements, intelligent transportation systems, numerical dosimetry, V2X.

The associate editor coordinating the review of this manuscript and approving it for publication was Valerio De Santis.

I. INTRODUCTION

A. OVERVIEW OF V2X WIRELESS TECHNOLOGIES

In recent years, wireless access technologies applied to connected and autonomous vehicles (CAVs) have emerged as a promising paradigm for enhancing safety, traffic efficiency, and reducing pollutant emissions through V2X communications. By improving situational awareness, optimizing traffic flow, and decreasing emissions, they have the potential to revolutionize transportation, leveraging communication between vehicles and all the other road actors (including pedestrians, signals, and infrastructures), through vehicle-to-vehicle (V2V), vehicle-to-infrastructure (V2I), vehicle-to-network (V2N), and vehicle-to-pedestrian (V2P) interactions. Consequently, Cooperative Intelligent Transport Systems (C-ITS) have evolved, supporting dynamic, real-time information exchange. This also provides solutions to challenges encountered in advanced autonomous driving technologies, such as perception blind spots, computational capacity limitations, and decision-making difficulties, thereby further advancing the development of intelligent transportation systems.

C-ITS systems are mainly enabled by two key wireless communication technologies: Cellular-V2X (C-V2X) and ITS-G5 (the European version of IEEE 802.11p) [1]. ITS-G5, derived from the Wi-Fi standard (IEEE 802.11) and also known as mobile Wi-Fi, operates at 5.9 GHz band with a typical Effective Isotropic Radiated Power (EIRP) of 23 dBm (0.2 W) and a maximum of 33 dBm (2 W), primarily facilitating short-range V2V and V2I communications. Meanwhile, the C-V2X technology, developed by the Third Generation Partnership Project (3GPP), encompasses LTE-V2X and 5G NR-V2X (released in 2018), supporting frequency range 1 (FR1) bands at 5.9 GHz (both LTE-V2X and 5G NR-V2X) and frequency rang 2 (FR2) bands (5G NR-V2X only), with a maximum EIRP of 23 dBm.

To implement C-ITS systems, various devices, especially RSUs and OBUs, have been developed. RSUs, as a critical component of vehicle-road cooperative technology, primarily gather road and traffic condition information and, through communication with roadside sensing devices, traffic signals, and electronic signage, allow real-time vehicle-road connectivity and traffic signal exchange, enhancing driving safety and efficiency. OBUs, on the other hand, engage in V2X communication with RSUs and can independently support various types of V2X communications, such as short-range V2V and V2I communication (ITS-G5), or connect to cloud services or traffic management centers via legacy cellular networks (C-V2X). It makes every connected car as a network node.

While the application of C-ITS and V2X technologies is expected to significantly improve road safety and traffic fluidity, the introduction of complex communication scenarios and new devices not only poses challenges for the development of communication technologies, such as channel modeling in high-speed mobility environments and electromagnetic compatibility issues [2], but may also lead to new health concerns. As C-ITS systems and V2X technologies could be widely deployed, road users will be continually exposed to EMF generated by various communication technologies, raising public concerns about the health impacts of EMF exposure in V2X communication scenarios.

B. LITERATURE REVIEW AND STUDY OBJECTIVES

To the best of the authors' knowledge, research on the level of EMF exposure for road users under V2X communication scenarios is currently limited. Existing studies have primarily focused on RF EMF exposure inside vehicles, centering on radiation sources from mobile communications and personal infotainment devices operating from 900 MHz to 2.5 GHz frequency bands [3], [4], [5], [6], [7], [8], [9], [10]. These studies do not encompass the novel frequency bands utilized in V2X communications and intelligent vehicular sensing devices, particularly ranging from 5.9 GHz to 24-80 GHz.

A preliminary work highlighting the importance of exposure studies at V2X frequencies has been proposed by Tognola et al. [11] and provides a comprehensive survey of RF EMF exposure from multiple technologies in connected cars, including V2X communication, automotive radars, and intra-car IoT devices. They discussed the frequency ranges, potential exposure levels, and compliance with existing exposure limits for each technology. The study highlights the necessity for an in-depth investigation into the real-world EMF exposure scenarios associated with 5.9 GHz V2X communications, particularly the lack of data on cumulative exposure effects when these systems operate concurrently with other technologies.

Regarding 5.9 GHz V2X technologies, there are studies [12], [13], [14], [15] that explore external antennas for V2V communication, focusing on antenna performance optimization and channel modeling, but they do not cover EMF exposure assessments in V2X connectivity. For example, Tognola et al. [1] employed numerical simulations to assess the Specific Absorption Rate (SAR) impact on vehicle occupants by roof-top antennas operating in the IEEE 802.11p technology's 5.9 GHz frequency band for V2V connectivity. The results indicated that, even in the worst-case exposure scenarios, the SAR values in various human tissues remained significantly below the ICNIRP's basic constraint. Schilling et al. [16] measured the electric field strength produced by ITS-G5, Bluetooth, and Wi-Fi technologies inside vehicles, finding that the maximum exposure level came from the ITS-G5 antenna on the front windscreen but did not exceed 15.1% of the ICNIRP reference level. Nevertheless, these studies mainly focused on the exposure levels inside vehicles without addressing the exposure assessment of pedestrians and others in V2X communication scenarios.

Recently, Bonato et al. [17], [18] conducted studies using numerical and stochastic dosimetry to investigate the electromagnetic exposure of pedestrians near vehicles equipped with 5G-V2X antennas operating at 3.5 GHz,

finding that even under the influence of antenna 3D beamforming, the SAR values in all evaluated scenarios remained below the basic restrictions for public exposure. In Benini's studies [19], [20], the EMF exposure of adults and children near vehicles with V2V technology has been assessed through simulation, considering two monopole antennas mounted on the roof operating at 5.9 GHz, reaching similar conclusions. In their most recent study [21], the authors employed ray tracing methods to simulate the EMF exposure levels (the Whole Body SAR (WBS) as metric) of road users in a simplified urban environment due to vehicles and infrastructure equipped with 5.9 GHz V2X antennas. The findings concluded that the WBS in this scenario was exceedingly low, generally around the level of 10^{-4} W/kg. Tognola et al. [22] used a hybrid deterministic and stochastic approach to evaluate the variability of RF exposure in urban V2V communication at the 5.9 GHz band across various human body models. The study revealed that even with multiple vehicles and antennas transmitting at maximum power, the median SAR values remained at lower levels. These studies highlight the application of numerical simulation in assessing EMF exposure but also point out the lack of experimental measurement data.

For the 24-80 GHz mmWave frequency band, commonly used in vehicles' Advanced Driver-Assistance Systems (ADAS) or Vehicle Occupant Detection (VOD) radar, there is currently a scarcity of research on the RF EMF exposure from vehicular mmWave radars in real-world scenarios. Existing studies on mmWave exposure include the work by Ruddle et al. [23], which assessed the exposure levels inside vehicles generated by external ADAS radars (24/46.8/77 GHz). It was found that the exposure produced by the highest frequency radar, 77 GHz, was a maximum of 0.76 W/m^2, well below the ICNIRP reference level of 10 W/m^2. Other studies [24], [25], [26] explored the temperature rise in eye and ear models under plane wave exposure in the mmWave frequency band through numerical simulation. Vermeeren et al. [27] measured the power density at distances of 3-30 mm from vehicle radars operating at frequencies of 60/79 GHz with maximum output power (10 dBm) and full duty cycle, finding that the antenna exposure levels (calculated as average power density) were below the basic limits set by ICNIRP. Thus, these studies have only analyzed exposure levels under highly simplified scenarios or laboratory environments. They have not conducted evaluations within actual vehicular contexts.

On the contrary, this study aims to comprehensively assess the impact of RF EMF exposure on road users when V2X communication technologies are adopted through a combination of numerical simulation and experimental measurement, thus filling the existing research gaps. Our research goals are multi-fold.

- First, we focus on assessing the impact of EMF radiation induced by ITS-G5 and C-V2X technologies employed by RSUs and OBUs on adults and children near RSUs,

FIGURE 1. RSU equipment: front view of the RSU at the left and its deployment on the highway at the right.

using numerical simulation methods with SAR values as the evaluation metric.
- Subsequently, we evaluate the exposure levels of RSUs in laboratory (in-lab) and real-world (in-situ) environments as well as OBUs installed on vehicles through experimental measurements of the electric field strength or EMF power density.
- Finally, our research measures the exposure levels of infotainment, advanced sensing, and IoT devices inside and around modern smart cars (with a Tesla Model S as the study object), with particular attention to Bluetooth, integrated LTE modules, and mmWave radar.

Through in-depth analysis, this study not only provides a scientific basis for understanding the levels of EMF exposure of V2X communication on road users but also serves as an important reference for the safe design and regulation of future intelligent transportation systems, promoting the safe application and development of intelligent transportation technologies.

The work is organized as follows: Section II details the simulation and measurement methods employed, Section III presents and comprehensively discusses the simulation and measurement results, and finally, Section IV summarizes the findings of this study.

II. EQUIPMENTS AND METHODOLOGIES
A. RSU EQUIPMENT SETUP AND RSU EXPOSURE SIMULATION
The RSU device involved in this study consists of a large electrical cabinet, which houses all the different modules of the RSU. These include modules for wireless communication, modules for local processing on the RSU, and modules that allow the RSU to be managed and recovered remotely when needed. The antennas of the communication modules are mounted on top of the RSU, as shown in Fig. 1 (left). The RSU is mobile, it can be installed outdoors during the testing period and positioned as desired in customs sites. Fig. 1 (right) shows one of the RSUs deployed along the E313 highway in Antwerp on top of the gantry.

Table. 1 lists the three commercially available wireless communication devices mounted on the RSU, including Cohda Wireless MK5 and MK6c, and Ettus USRP N310 (a Software Defined Radio (SDR), hereafter referred to as SDR), along with their respective implemented

TABLE 1. Characteristics of the wireless communication devices and their technologies implemented on the RSUs.

Device	Technology	Relevant standard	Frequency band (GHz)	Channel bandwidth (MHz)	Data rate (Mbps)	Max Tx EIRP (dBm)
Cohda MK5 [28]	ITS-G5	IEEE std 802.11p [29] ETSI EN 302 571 [30]	5.855 - 5.925	10 / 20	6 / 12	33
Cohda MK6c [31]	C-V2X Through PC5[a]	ETSI EN 303 613 [32] 3GPP TR 36.885 [33] ETSI TS 136 101 [34]	5.855 - 5.925	10 / 20	6 / 12	23
Ettus USRP N310 (SDR) [35]	C-V2X Through Uu[b]	3GPP TR 38.886 [36] 3GPP TR 38.785 [37]	LTE band: 0.8, 1.8, 2.6 FR1 band: 3.5 ITS band: 5.855 - 5.925	100	-	23

If not explicitly indicated, the max allowed transmitted EIRP power (Max Tx EIRP) set by the standards is calculated as A + G + 10 log (1/DC), where A (dBm) is the measured power output of the device, DC is the duty cycle, and G is antenna assembly gain (dBi).
[a]The PC5 interface is a short-distance direct communication interface for V2V, V2P, V2I, and includes the communication interface between RSUs and OBUs.
[b]The Uu interface enables long-distance, high-speed data transmission between the terminal (RSU/OBU) and the base station.

communication protocols, especially noting their maximum transmitted ERIP power which will be used in our subsequent simulations and experimental measurements. It is evident that RSU's technology stack covers the current mainstream V2X communication technologies. It is important to note that while the ITS-G5 technology implemented by Cohda MK5 specifies a maximum transmitted EIRP power of 33 dBm (for non-government services), the actual maximum transmission power of this device is only 23 dBm. The maximum transmission power of Cohda MK6c is 23 dBm, consistent with the standard specification of the C-V2X technology (Table. 1). The SDR implementation of C-V2X technology through the Uu interface, including LTE-V2X and 5G NR-V2X technologies, has not been deployed in real-world RSUs. Therefore, no related measurements of this device were involved in experimental measurements. However, in the numerical dosimetry investigation, the SDR's transmitting antennas for each band (as specified in Table. 1) are still included as radiation sources in this work to consider the worst-case scenario.

As far as the simulation is concerned, the exposure scenarios are illustrated in Fig. 2. It includes an overall model of the RSU, consisting of an electrical cabinet, a base plate for mounting antennas of each communication module, and a human body model (adult or child) placed sequentially at four marked positions, which namely: "POS 1", "POS 2", "POS 3", and "POS 4". Specifically, we considered two types of Virtual Population (ViP) anatomical human models, namely the Duke model (an adult male, 34 years old) [38] and the Billie model (a female child, 11 years old) [39].
Fig. 2 also depicts the layout of the transmitting antennas, it includes three ITS 5.9 GHz antennas: the Cohda MK5 (ITS-G5), Cohda MK6c (C-V2X, PC5 Interface), and SDR N310 (C-V2X, Uu Interface), which are denoted by blue, green, and yellow circles, respectively. Additionally, the RSU's SDR is connected to antennas operating at other frequencies. This includes two tri-band antennas for LTE technology operating at 0.8, 1.8, and 2.6 GHz, marked with green triangles, and a 5G NR FR1 band antenna at 3.5 GHz, indicated by a
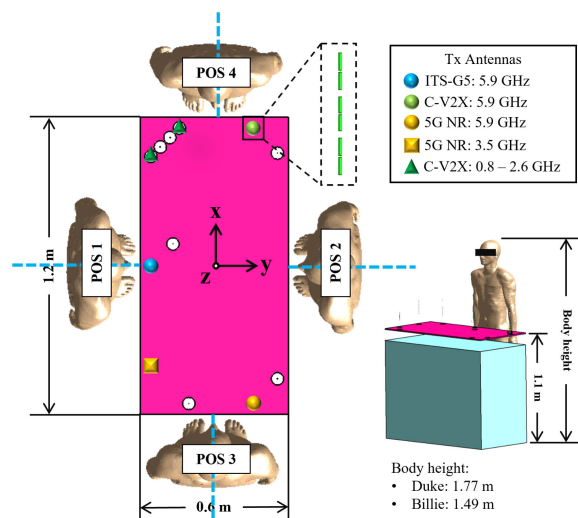

FIGURE 2. Simulation scenario: a full RSU setup, featuring all the transmitting antennas, with tri-band: 0.8-1.8-2.6 GHz (marked as triangles), 3.5 GHz (square), and 5.9 GHz (circles) antennas for each technology, along with a human model (Duke or Billie) placed beside each of the RSU's four sides.

yellow square. An active Global Navigation Satellite Systems (GNSS) antenna is also connected, although it is not modeled in this study due to its irrelevance to our study.

The simulations were conducted by Sim4life (ZMT Zurich Med Tech AG, Zurich, Switzerland) [40], which utilizes the Finite-Difference Time-Domain (FDTD) method for its solver. The antennas installed on the RSU were modeled as dipole arrays matching the dimensions of commercial antennas actually used in practice (an example of a modeled 5.9 GHz antenna is depicted in Fig. 2), with antenna and electrical cabinet materials set as perfect electric conductors (PEC) to enhance simulation speed; the base plate was modeled with plexiglass (relative permittivity $\varepsilon_r = 2.6$ and conductivity $\sigma = 0.0025$ S/m). The excited antenna's terminal was set with a 'single edge' voltage source (input voltage of 1V) with an internal reference impedance of

50 Ω, whereas the terminals of the remaining antennas not fed were set with a lumped load of 50 Ω. The adult and child human models used the ViP v.3.0 Duke [38] and ViP v.1.0 Billie models [39] respectively, with the dielectric properties (ε_r and σ) of different tissues at the frequencies of each transmitting antenna were assigned according to [41], and each human model was meshed with a step size of 1 mm. The boundary of the simulation computational domain was enclosed with 6 layers of Perfectly Matched Layers (PML), and the convergence condition was set to -50 dB to balance simulation accuracy and computation time.

To compare with the results of experimental measurements, we first calculated the spatial electric field within 2 m around the RSU on the azimuthal plane (i.e. E-plane of the antennas) of the antennas with both Cohda MK5 and MK6c switched on, excluding the human model. Both ITS-G5 and C-V2X utilize Orthogonal Frequency Division Multiplexing (OFDM) and Quadrature Amplitude Modulation (QAM) modulation, meaning that the signals transmitted by the two antennas are not always in phase; the phase difference varies randomly over time. This leads to fluctuating exposure patterns from the two antennas. To better understand the variations in EMF exposure levels due to multi-signal source interactions, we set the phase of one antenna's source to 0° and varied the phase of the other from 0° to 360° (excluding 360°), at intervals of 45°, including randomly selected intermediate values, resulting in 16 distinct phase differences: 0° (in phase), 21.9°, 45°, 66.2°, 90°, 107.6°, 135°, 167.4°, 180°, 205.6°, 225°, 246.2°, 270°, 290.2°, 315°, and 338.4°. All results normalized to their actual transmission power of 23 dBm.

For dosimetric assessment, simulations at each frequency were conducted with all antennas transmitting at that frequency activated at the same input power and in phase to simulate the worst-case scenario. Following the guidelines of the ICNIRP [42], the simulations calculated the peak spatial-average SAR averaged over 10 g (psSAR$_{10g}$) of tissue and the WBS, across all frequency bands implemented by the RSU at four specific positions. Specifically for the 5.9 GHz frequency band of interest in this study, the SAR$_{10g}$ distribution was calculated and analyzed within six typical human tissues: skin, subcutaneous adipose tissue (SAT), fat, muscle, bone, and blood. These results were normalized to an input power of 1 W (EIRP: 30 dBm) for convenience in rescaling the SAR values at different input powers.

B. RSU AND OBU EXPOSURE MEASUREMENTS SETUP

For the experimental measurement of EMF exposure levels from RSUs and OBUs, we measured the root mean square (RMS) value of electric field strength E in V/m (or the power density S in W/m^2) of the received signals. The equation for the interconversion between S and E is [42]:
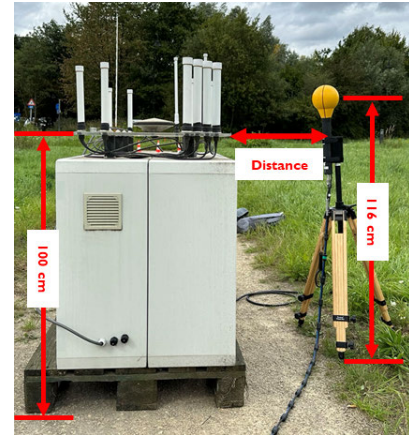
$$S = \frac{|E|^2}{Z_0} \qquad (1)$$

FIGURE 3. RSU in-lab measurement experiment setup. The probe, positioned 1.16m above the ground, is placed at various distances around the four sides of the RSU.

where Z_0 is the characteristic impedance of free space, i.e., 120π Ω. To this aim, we used a Narda SRM3006 Spectrum Analyzer (SA) and an isotropic Narda 420 MHz-6 GHz triaxial antenna (probe) with a measurement uncertainty of ±3 dB in isotropic measurement mode.

The exposure levels of the RSUs have been evaluated both in laboratory (in-lab) settings and on-site next to the highway (in-situ). Fig. 3 shows the in-lab measurement setup. Precautions were taken to avoid pedestrians to prevent any impact on the measurements. The measurement points were aligned to the simulation, situated in the directions of the four sides of the RSU. The center of the probe was positioned at a height of 1.16 m above the ground, and the distance between the probe and the RSU was defined as the distance from the center of the probe to the edge of the RSU antenna base plate. The measurement points in each direction from the RSU were at distances of 0.5 m, 1 m, and 2 m. It is important to highlight that we configured all the devices to transmit continuously to allow us to measure the worst-case conditions, so both MK5 and MK6c were configured to continuously transmit their real-time Global Positioning System (GPS) information at a bandwidth of 10 MHz, maximum byte rate of 12 Mbps, and maximum transmit power of 23 dBm during the measurements.

For in-situ measurements alongside highways where RSUs are deployed, the upper part of Fig. 4 shows seven RSUs positioned along the E313 highway in Antwerp as part of the Smart Highway testbed for developing C-ITS applications [43]. The wireless communication modules installed in these RSUs and their technical characteristics are identical to those used in the RSU for the in-lab experiments described in this study and thus are not reiterated here. In this work, we selected two of these seven deployment sites for evaluating the exposure levels in the vicinity of their RSUs, hereafter referred to as Site 1 and Site 2, respectively. The lower part of Fig. 4 depicts the RSU at Site 1 and its installation position on the gantry top along

FIGURE 4. RSUs deployment along the E313 highway in Antwerp (upper) and RSU used for measurements and its installation position on the top of a gantry (lower).

the E313 highway. We used the Duke human model from the ViP [38] as a reference to define the measurement positions. We selected measurement points at heights of 1 m (basin (pelvis) position) and 1.64 m (eye level) above the ground, as well as the maximum height reachable by the probe at 2 m. At Site 1, the exposure levels at these points were measured at distances of 1 m, 5 m, and 10 m from the gantry. Conversely, at Site 2, the scope of measurement was expanded, conducting continuous measurements at six positions extending from 13 m away from the gantry, which was installed with RSU, approximately every 9 m. Still, vertical measurement points were confined to heights of 1 m and 2 m. For both in-lab and in-situ measurements, the SA was set to frequency domain measurement (default mode) in max-hold mode (with RMS detector) to record the highest field levels received until the signal stabilized. Fig. 5 (a) and Fig. 5 (b) respectively present the experimental setups for the in-situ measurements conducted at Site 1 and Site 2.

Furthermore, we dynamically assessed the exposure levels at passenger seats in vehicles traveling on highways equipped with RSUs (so-called on-road measurements). Specifically, vehicles were driven past two RSUs with the SA probe placed in the passenger's seat at a height of approximately the human chest. Fig. 5 (c) depicts the setup of this on-road in-car experimental measurement. In Fig. 5 (c), the gray car was equipped with an OBU antenna on the roof, but this OBU was only used to verify the RSU's work status in this experiment and was not used for signal transmission.

Critically, all in-situ measurements were preceded by a control measure, where all wireless communication devices on the RSU were turned off to observe the spectrum of our measured band and ensure no signals from other radiation sources were present. All in-situ measurements were conducted in full compliance with local traffic safety laws and regulations.

This study also assessed the exposure levels from a Cohda MK5 OBU based on ITS-G5 technology, aiming to measure the electric field or power density received both outside and inside the vehicle. Measurements used an Audi A5, where the Cohda MK5 OBU installed shared the basic characteristics with the Cohda MK5 on the RSU, with the difference that the OBU's maximum transmission power could be set to the maximum transmission power of 33 dBm following ETSI standard [30]. Hence, to accommodate worst-case scenarios, all our measurements were conducted with the OBU transmitting at this power level. The OBU was equipped with a shark fin antenna such that the transmitted EIRP was equal to 33 dBm with a gain of 5 dBi. As shown in Fig. 6 (a), we considered two antenna configurations, symmetrically placed on the vehicle's roof at the front and rear windscreens proximity, indicated by the blue dots in the figure. To comprehensively measure the electric fields received from the front/rear antenna both outside and inside the vehicle, we predefined five measurement positions each for the exterior and interior. For the exterior, the five positions and their respective distances from the front/rear antenna are also indicated in Fig. 6 (a). Similar to the RSU's in-situ measurements, we referenced the Duke and Billie models from the ViP model for positioning the probe at the height of the head (eye) and basin (pelvis) for measurements, with Fig. 6 (a) also showing these heights. As for the in-car measurements, shown in Fig. 6 (b), the predefined positions were determined based on the five passenger seats within the vehicle cabin, namely: driver, front passenger, back left, back central, and back right seat. At each seat, electric field strength was measured at both the head and basin positions (Fig. 6 (b)).

C. TESLA DEVICES MEASUREMENTS SETUP

In this study, we investigated the exposure levels inside and around a modern smart vehicle (Tesla Model S) from Bluetooth technology used by infotainment devices, integrated LTE wireless communication technology, and mmWave radars used by advanced sensing systems. The locations of the exposure sources of the various technologies installed on the investigated vehicle are illustrated in Fig. 7 (a). This work involved measuring the electric field strength/power density and DC (%) of the signals emitted by these technologies, with DC defined as the fraction of the actual transmission time of these signals t_{trans}(s) to the total measurement time t_{tot}(s) [44], [45]:

$$DC = \frac{t_{trans}}{t_{tot}} \times 100 \; (\%). \qquad (2)$$

For this purpose, we followed the measurement procedures outlined by [46] and [47]. Specifically, two types of mmWave radars are mounted on the Tesla Model S; one located above the car's front lights, performing Long Range Radar (LRR) protocol for long and short-range detection applied in ADAS; the other radar, intended for occupant detection and potential driver awareness, i.e., VOD applications and located near
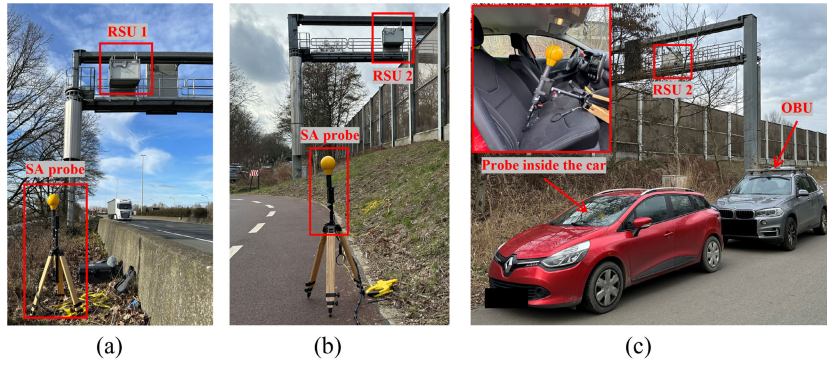
FIGURE 5. The RSU in-situ static measurement setups at (a) Site 1, (b) Site 2, and (c) the on-road in-car measurement setup.
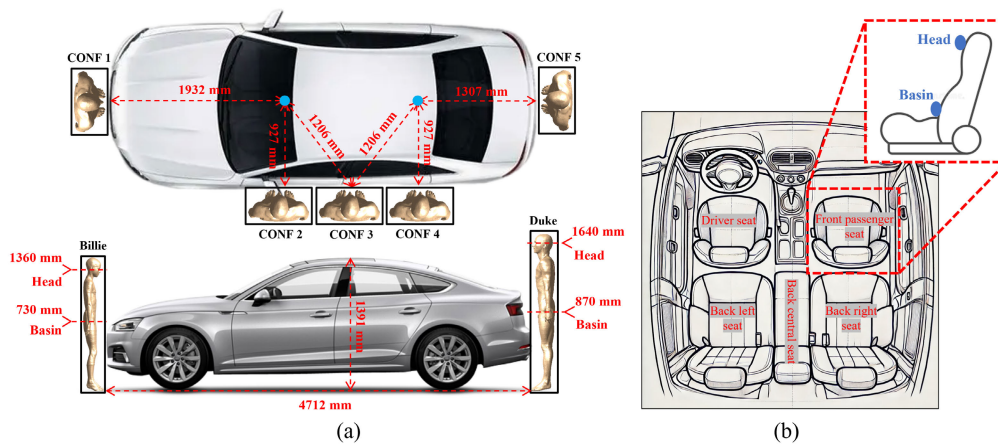

FIGURE 6. OBU measurement setup: (a) two blue dots on the car roof indicate the two OBU antenna positions; five predefined measurement positions around the car, labeled CONF 1-5, along with the distances from each position to the two antenna; the lower part of the figure shows the heights from the ground for the four measurement points based on the ViP Duke and Billie human models. (b) illustrates the five seats inside the vehicle and the defined measurement points at each seat (i.e., 'Head' and 'Basin').

the front interior ceiling, was not activated according to information provided by the manufacturer and hence was disregarded, focusing only on the radar located at the front light (Fig. 7 (a)). Accordingly, frequency domain (default mode) measurements to determine its operating frequency band and zero-span temporal measurements to measure its signal amplitude and DC were conducted following [46], using an FSV-3030 (SA) and a mmWave probe (Mi-Wave 267V omnidirectional antenna [48]) for measurements. We placed the mmWave probe 20 cm away from this radar (front light), the setup is shown in Fig. 7 (b). It is noted that the SA and probe used for measuring the technologies at relatively lower frequencies (Bluetooth and LTE) were consistent with those used in the RSU/OBU experimental measurements.

We measured the electric field strength and DC of the Bluetooth devices inside the vehicle under different operating states. It should be noted that while the tire pressure sensors are equipped with Bluetooth Low Energy (BLE) modules, their transmission only occurs when the tires are rotating,

thus their measurement was omitted. This study considered the electric field levels received at the driver and passenger positions under different operating modes of the Bluetooth device, i.e., when the vehicle is turned off, idle, searching, and when connected to a phone transmitting data continuously (playing Spotify). To this aim, the probe was placed at the torso positions of the driver and passenger, as illustrated in Fig. 7 (c). Notably, when the Bluetooth device was connected to a phone for continuous data transmission, the phone was placed between the two seats, measuring the EMF exposure levels from both the vehicle's Bluetooth and the phone's Bluetooth simultaneously.

Finally, we measured the exposure level from the vehicle's integrated LTE communication module, with its antenna integrated inside the rearview mirror housing, as shown in Fig. 7 (a). We considered two states of the vehicle: turned off and startup. In the initial measurement, the probe was directly in contact with the rearview mirror housing (probe diameter: 12 cm), referred to as the 0 cm distance. Subsequent measurements were taken at distances of 15 cm and 50 cm
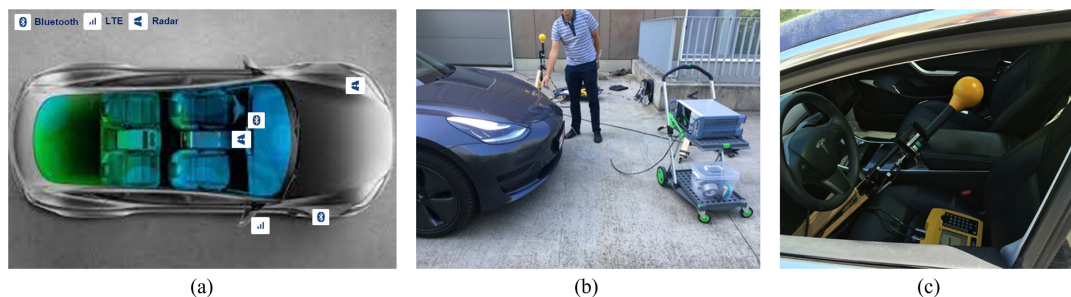
FIGURE 7. (a) Top view of Tesla Model S and position of each wireless communication device under investigation; (b) measurement setup for the radar in the headlights, involving an FSV-3030 SA with a mmWave probe held very close to the radar; (c) measurement setup for the in-vehicle Bluetooth device, involving an SRM3006 SA and a probe placed on the height of the chest of the driver.

from the rearview mirror to measure the electric field strength and DC of the signals emitted by the module.

III. RESULTS AND DISCUSSION

A. RSU MEASUREMENTS AND SIMULATIONS

To the best of the authors' knowledge, this study represents the first assessment of human RF EMF exposure in V2X communication scenarios implemented with ITS 5.9 GHz technology within RSU-based V2I cooperative systems. We conducted numerical simulations, in-lab, and in-situ measurements. An RSU with 5.9 GHz, LTE, and 5G NR antennas was modeled using FDTD to calculate the electric field, which was then validated by in-lab measurements. Exposure levels were evaluated using ViP anatomical models (Duke and Billie) for SAR_{10g} and WBS. In-lab and in-situ experiments measured exposure at various distances from the RSU.

Fig. 8 shows the electric fields around the RSU as a function of distance in every 4 directions along the blue dash line showed in Fig. 2 extracted from simulation results, alongside the exposure levels at different distances measured in the in-lab experiment. Fig. 8 illustrates the simulation results with three curves showing the electric field distribution: one for ITS-G5 and C-V2X antennas under in-phase excitation, and the other representing the maximum and minimum field distributions obtained with different phase differences between the two antennas. Simulation results revealed that in the POS 1 and POS 2 areas, the in-phase excitation produces the highest field strength among the 16 different phase shifts tested. Conversely, in the other areas, there are configurations with different phase differences that result in higher field levels. Focusing on the maximum field strength distributions obtained from the simulation, in the reactive near-field region close to the antennas, the field strength is higher with noticeable fluctuations. However, the field rapidly decreases as the distance from the antenna increases, especially at POS 3 and 4, reaching up to 20 V/m within 0.5 m from the RSU but then quickly dropping below 5 V/m and continuing to decrease inversely with the square of the distance. In the study by Tognola et al. [1], FDTD simulation was used

to assess the exposure level to occupants inside a vehicle from ITS-G5 technology operating at 5.9 GHz in terms of SAR within the human body. Although the transmission power, antenna types, antenna installation positions, and exposure scenarios used in [1] are different from ours, making a direct quantitative comparison unfeasible, a qualitative observation can be made that the field generated inside the vehicle by an ITS-G5 monopole antenna mounted on the vehicle's exterior also decreases very rapidly with distance, showing a more significant attenuation rate compared to other communication technologies operating at lower frequencies (LTE, Bluetooth, etc., operating frequencies within 0.8-2.6 GHz). This indicates the relatively higher path loss of this frequency band. Despite the absence of transmitting antennas near POS 1 and 2, the field is maximally superimposed at these two positions due to the symmetrical distribution of the two antennas relative to these positions. Even though the exposure level is not as high as at POS 3 and 4 within close proximity to the RSU (within 0.5 m), the overall decreasing trend is not as rapid, hence the highest exposure level measured in the in-lab experiment was 5.8 V/m at POS 1, 0.5 m from the RSU. It can also be seen that although other antennas of different frequency bands are installed on the RSU, their impact on the field at POS 3 and 4 at 5.9 GHz can be disregarded, with the electric field at these positions being considered symmetrically distributed.

Fig. 8 also presents the in-lab measurement results of exposure levels (RMS values of the electric field) at different distances around the RSU, with the uncertainty of isotropic measurements: ±3 dB displayed as error bars in the figure. As mentioned, the highest measured exposure level was 5.8 V/m, which is 9.5% of the ICNIRP's reference level of 61 V/m for the 5.9 GHz field. Comparing simulation and in-lab measurement results reveals good agreement, particularly at distances of 1 m and 2 m from the RSU in various directions. However, field strength measurements at 0.5 m from the RSU are consistently lower than those predicted by simulations, most notably in the POS 3 and POS 4 regions, with deviations not exceeding 3 dB in the POS 1 and POS 2 regions, which remains within a reasonable range. Three primary factors contribute to these deviations:
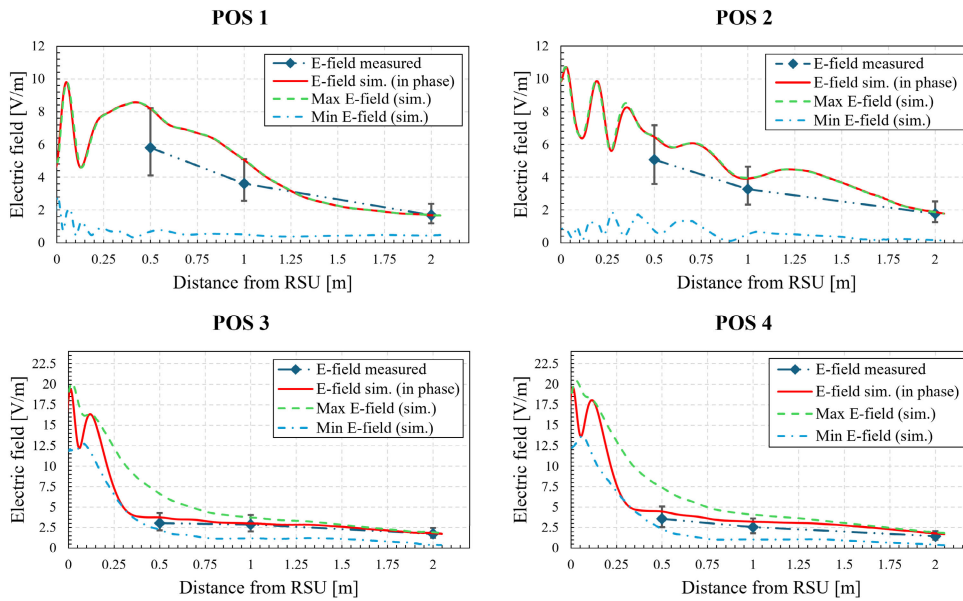
FIGURE 8. Simulated (normalized with input power of 23 dBm) versus measured (input power of 23 dBm) electric field (RMS value) generated by the RSU antennas as a function of the distance from the antenna. The simulation results present three curves: one for ITS-G5 and C-V2X antennas under in-phase excitation, and two representing the maximum (Max E-field) and minimum (Min E-field) field distributions with varying phase differences between the antennas.
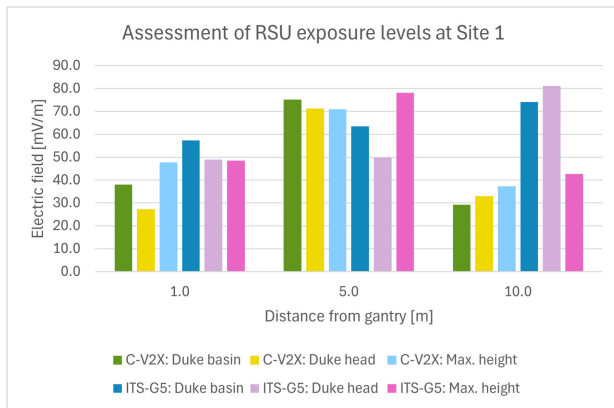

FIGURE 9. Site 1 RSU measurements: Electric field (RMS value) of ITS-G5 and C-V2X (both with 23 dBm input power) as a function of distance for three heights: 1 m ("Duke Basin"), 1.64 m ("Duke Head"), and 2 m ("Max. Height").

FIGURE 10. Site 2 RSU measurements: Electric field (RMS value) of ITS-G5 and C-V2X (both with 23 dBm input power) as a function of distance for two heights: 1 m and 2 m.

firstly, the phase differences in signals causing significant exposure are transient, and our use of an RMS detector to prevent systematic overestimation of exposure levels results in the under-recording of higher field strengths; secondly, there is uncertainty in the placement of the measurement probe; and lastly, differences between the simulated and actual commercial antennas used, as well as the uncertainty in the input power of each device.

Fig. 9 presents the in-situ static measurement results at Site 1 for ITS-G5 and C-V2X technologies at three different heights selected with reference to the ViP Duke human model, showing the exposure levels at various distances from
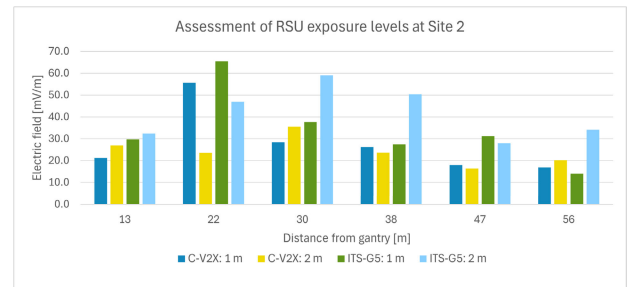
the gantry equipped with the RSU. It is observed that due to the far-field pattern of the antennas, i.e., the omnidirectional dipole (array) antenna, the closest position to the RSU in the horizontal direction, specifically 1m from the gantry, is not where the highest exposure level is found since this position is almost immediately below the RSU. Similarly, the closest vertical position to the RSU does not always correspond to the highest exposure level. For the ITS-G5 technology, the maximum exposure level was measured at 81.2 mV/m at the eye level of the Duke human model (i.e., Duke Head, 1.64 m) 10 m away from the gantry, significantly below the ICNIRP's reference level of 61 V/m, representing less than -58 dB of the reference value. For C-V2X technology, the position of the maximum exposure level was found at 5m from the gantry at the basin region of the human model (Duke Basin, 1 m), measuring 75.2 mV/m, also not exceeding -58 dB of the ICNIRP reference level.

Fig. 10 presents the exposure levels measured at Site 2 for two technologies. Considering the measurement results from both sites, it becomes clear that the exposure levels of both technologies do not monotonically decrease with increasing distance from the radiation source. Instead, significant fluctuations were observed at some locations, with the maximum variation exceeding 8 dB between two adjacent measurement points at the same height, and a maximum difference of 7.7 dB between two measurement points at different heights but the same horizontal position. This reflects that due to their higher frequency (5.9 GHz), the spatial variation in exposure levels for both technologies is pronounced, and the complexity of real-world RF propagation. Nevertheless, the overall trend shows a decay in exposure levels with increasing distance, with the maximum exposure level measured at Site 2 (65.5 mV/m) being lower than that at Site 1, but the rate of decrease is not linear, which could be due to environmental factors, interference, or multi-path propagation effects.

For the real on-road in-car measurements, the maximum exposure levels recorded at the passenger position for ITS-G5 and C-V2X technologies were 12.4 mV/m and 10.3 mV/m, respectively, which is 74 dB lower than the ICNIRP reference level (61 V/m). It is important to note, as mentioned in [49], that the number of occupants inside the vehicle can affect the exposure levels. The experiment included two occupants in the vehicle, including the driver.

Since the SAR values are directly proportional to the input power, we normalized the calculated human SAR values for an antenna transmit power of 1 W. This normalization facilitates the scaling of SAR values for different input powers. Table. 2 shows that the highest $psSAR_{10g}$ in both Duke and Billie occurs when the human body is positioned at POS 4, exposed to the 2.6 GHz electric field. This is due to the fact that the human body is the closest to the transmitting antenna (LTE band 0.8-2.6 GHz antenna, marked as the green triangle in Fig. 2) at this location. The maximum $psSAR_{10g}$ values for the two cases are 248.7 mW/kg (Duke) and 218.5 mW/kg (Billie), respectively, both are 8 times below the 2 W/kg limit of local exposure (torso) in the 100 kHz-6 GHz range set by ICNIRP. Nevertheless, the maximum transmit power in this 2.6 GHz LTE band is limited to 23 dBm, so the results here normalized to an input power of 1 W overestimate the SAR. Rescaling the results by the EIRP of 23 dBm, the values of the two maximum psSAR10g above become 49.7 mW/kg and 43.7 mW/kg, respectively, which is 40 times lower than the ICNIRP limit.

For the ITS 5.9 GHz band of interest in this study, we analyzed the SAR_{10g} distribution in human tissues at this frequency. Fig. 11 compares the distribution of SAR_{10g} in various tissues (Skin, SAT, Fat, Muscle, Bone, and Blood) within the two human models (Duke and Billie) across different exposure scenarios at 5.9 GHz. It is important to note that SAR averaging is generally considered an average over a cubical mass of tissue. However, for thin-layered tissues (e.g., skin), the averaging volume may substantially deviate from a cube due to the complex algorithm used for

TABLE 2. The $psSAR_{10g}$ and WBS (normalized with input power of 1 W) for the human models (Duke and Billie) calculated in each RSU exposure scenario.

Exposure scenario		$psSAR_{10g}$ (mW/kg)		WBS (mW/kg)	
Position	Frequency (GHz)	Duke	Billie	Duke	Billie
POS 1	0.8	24.29	16.09	0.24	0.33
	1.8	84.33	78.55	1.31	1.79
	2.6	22.33	19.35	0.13	0.48
	3.5	90.89	73.22	0.78	1.05
	5.9	78.29	99.47	0.49	1.06
POS 2	0.8	6.42	9.94	0.48	0.79
	1.8	13.74	34.13	0.58	0.95
	2.6	17.59	39.35	0.43	0.95
	3.5	37.67	27.10	0.55	0.72
	5.9	23.07	20.70	0.13	0.16
POS 3	0.8	1.19	1.38	0.10	0.16
	1.8	8.82	8.88	0.15	0.26
	2.6	43.59	46.15	0.63	0.98
	3.5	96.65	85.16	0.90	1.21
	5.9	90.95	84.99	0.60	0.57
POS 4	0.8	36.44	28.46	0.47	0.85
	1.8	150.56	178.76	1.85	3.60
	2.6	248.68	218.51	1.59	2.07
	3.5	5.39	5.78	0.06	0.06
	5.9	73.62	92.75	0.51	0.76

SAR averaging [50]. The results in Fig. 11 show that the distribution of SAR_{10g} in all scenarios and tissues exhibits a positive skewness, meaning that in various scenarios, the SAR_{10g} values for most tissues are distributed at lower exposure levels, with only a few samples reaching relatively high SAR_{10g} values. In all exposure scenarios, the skin obtains the highest SAR_{10g} values, significantly higher than those of other tissues, i.e., the radiation energy was predominantly absorbed by the skin. The maximum values occur when Billie is at POS 1 and Duke at POS 3 (Fig. 2), with 264 mW/kg and 223 mW/kg respectively, both considerably below the ICNIRP's basic restriction for general public exposure of local SAR_{10g} (torso), which is 2 W/kg [42]. These positions also represent the closest proximity of the two human models to the antenna. Fig. 12 shows the distribution of SAR_{10g} over the skin of the whole human models in each exposure scenario at 5.9 GHz, normalized by their peak values. Due to differences in body height, for Duke, the SAR_{10g} is primarily distributed in the abdominal area, whereas for Billie, it is mainly in the chest region. Finally, Table. 2 lists the WBS for different human body models in each exposure scenario. The maximum WBS at 5.9 GHz for Duke and Billie are 0.60 mW/kg and 1.06 mW/kg, respectively, which are both below the 0.08 W/kg limit for the general public exposure [42] (-18 dB of the ICNIRP). Additionally, in most exposure scenarios, Billie's WBS is higher than Duke's despite Billie having a smaller body volume. This is because, although Billie absorbs slightly less EMF power compared to Duke, the difference in energy absorption is smaller than the difference in weight between Billie and Duke, resulting in higher WBS for Billie.
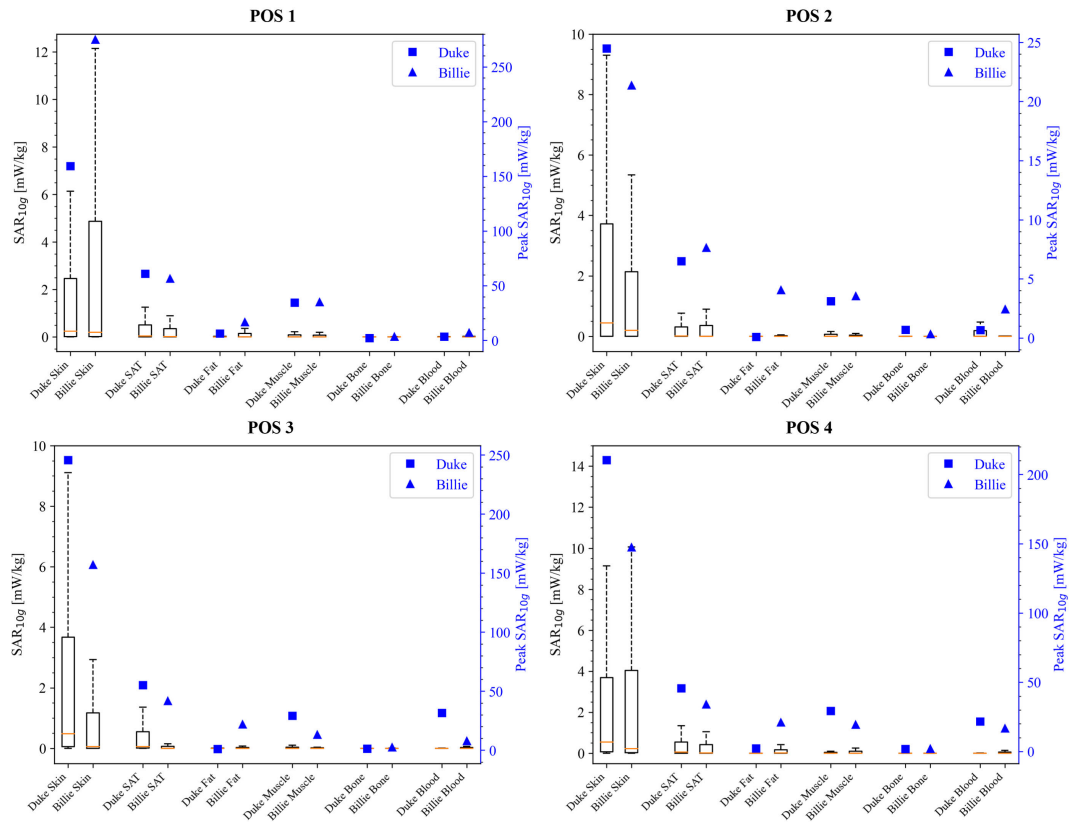
FIGURE 11. Box plot of the 10g average SAR (normalized with input power of 1 W) distribution in each tissue (skin, SAT, fat, muscle, bone, and blood) of the two human models for the four exposure scenarios at 5.9 GHz. The orange line in the center of the box indicates the median; the top and bottom edges of the box represent respectively the 75th and 25th percentiles; the upper whisker is 1.5 times the height of the box i.e. 99.3% of 10g average SAR value, the lower whisker is the minimum value.

Comparing our results with prior studies helps to establish a clearer picture of the exposure in the V2X communication scenario. Although recent studies have primarily focused on exposure assessments within V2V, i.e., OBU communication scenarios, they all utilize ITS-G5/C-V2X technologies. By cross-comparing exposure levels across different endpoint devices within V2X communication scenarios, we can gain a more intuitive understanding of the exposure levels of RSUs, especially in relation to OBUs. Therefore, conducting a qualitative comparison of these studies is meaningful. In a recent study, Benini et al. [21] employed the ray tracing method to simulate exposure assessments in urban environments, using WBS as a metric. Their research utilized a simplified city model and five vehicle models, with 5.9 GHz antennas having a gain of 0 dBi (i.e., half-wave dipole) and a maximum transmission power of 33 dBm. They found that the exposure levels were generally very low (on the order of 10^{-4} W/kg), even in the worst-case scenario where antennas on five vehicles and traffic light RSUs were transmitting simultaneously, the maximum WBS was only $4.9 \cdot 10^{-4}$ W/kg, far below the ICNIRP limits. Due to the human models being further from the transmitting antennas compared to this study—at least 8 m away—and the lower antenna gain, the

calculated exposure levels were much lower than those found in our research.

Other studies by the same authors [19] and [20] conducted numerical dosimetry assessments of electromagnetic exposure levels for adults and children near vehicles equipped with 5.9 GHz antennas for V2V connections. In these studies, two monopole antennas identical to those in [1] were placed at the front and rear positions on the vehicle roof, each with an input power of 1 W, the same as in our study. Different human models were positioned around the vehicle in two orientations. The highest local SAR_{10g} values were likewise found in the skin tissues, with the adult model (Ella) having a maximum SAR_{10g} in the head skin tissue of 34.7 mW/kg, and for the child model (Dizzy), it was 9 mW/kg. Both are below the maximum SAR_{10g} values found in adult and child skin tissues exposed to the 5.9 GHz RF field in our study. The reasons are twofold: firstly, although the human models in [19] and [20] were placed very close to the vehicle, the shortest horizontal distance from the models to the actual antenna installation positions was still 0.5 m, especially the child model, which due to its shorter stature, was further from the antennas, overall greater than the distance between the human models and the antennas in this study; secondly,
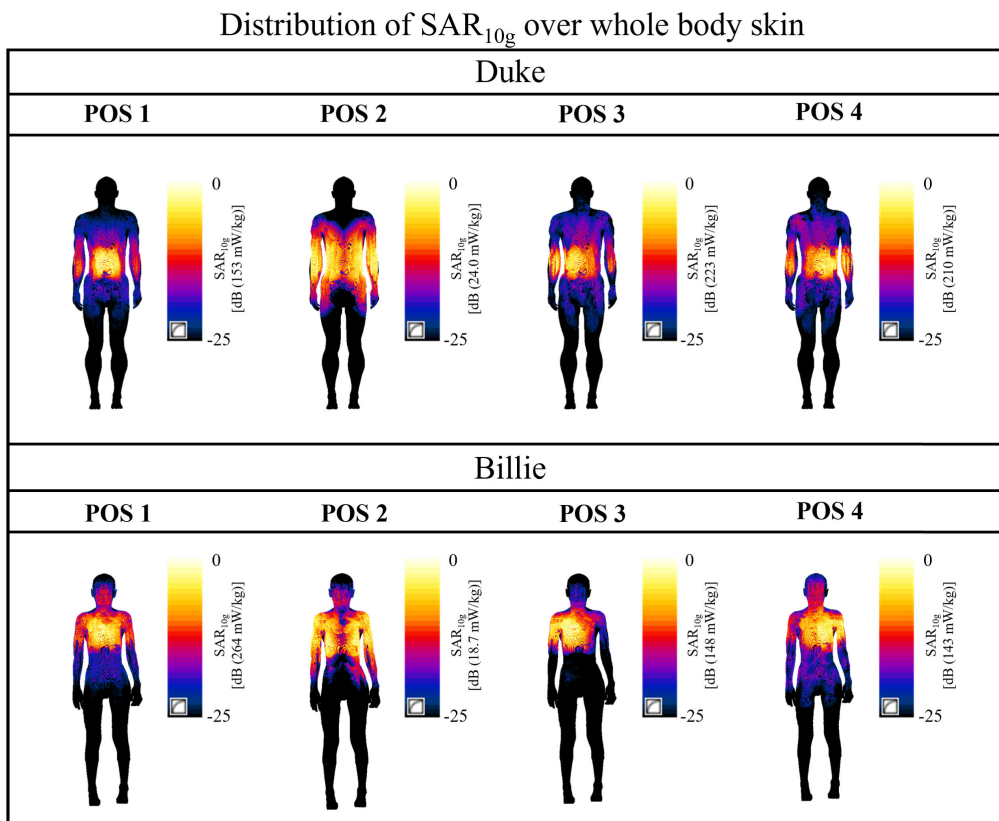
FIGURE 12. Distribution of normalized 10g average SAR across the whole body skin of different human models (Duke and Billie) for each RSU exposure scenario at 5.9 GHz (normalized to their respective maximum values). Color map range from 0 to -25 dB.

compared to the two independent monopole antennas in [19] and [20], each transmitting antenna in this study consists of an array of three dipoles, offering higher directionality and gain towards the human models. For WBS, the maximum values in [19] and [20] for adult and child models were 0.19 mW/kg and 0.18 mW/kg, respectively. These values are not only lower than those found in our study but also indicate that the WBS for children is less than for adults, due to the lower height of children causing them to be further away from the antennas compared to the adult model.

In [1], an ''asymmetric'' worst-case exposure scenario was considered, moving the originally symmetrically mounted antennas on the vehicle roof and rear/left mirrors directly to the nearest point to the head of the human model inside the vehicle and simultaneously activating these four antennas with the maximum transmission power of 44.8 dBm (30 W) as specified by the IEEE 802.11p protocol (for U.S. government services). They found the maximum local SAR_{10g} in the head's skin issue to be 1.58 W/kg, and the WBS to be 0.008 W/kg. Scaling our results to the input power of 30 W, the values for the adult model become 6.7 W/kg and 0.018 W/kg, respectively; for the child model, they would be 7.9 W/kg and 0.032 W/kg. Hence, the local exposure levels in our findings not only exceeded those in [1] but also surpassed the general public exposure limits set by ICNIRP [42] and IEEE [51], while the WBS remains

below the limit and is higher than in [1]. Although [1] used four antennas, in the ''asymmetric'' scenario, only two antennas were within 0.5 m of the human model, and the vehicle's metal body (PEC) partially shielded the occupants. It is noteworthy that these local exposures exceeded general public exposure limits because they used the maximum transmission power reserved for government services, and such close proximity between the human body and the RSU typically occurs in occupational exposure scenarios. Fig. 4 shows an example of a real RSU deployment location, situated at the top of gantries, a position inaccessible to pedestrians. Therefore, assessing them against occupational exposure limits is more reasonable, and these local SAR values are all below the ICNIRP and IEEE occupational limits (for the torso), which is 10 W/kg. Moreover, if these antennas were implemented with C-V2X technology (including 5G-V2X), with the protocol's maximum input power set at 0.2 W (EIRP: 23 dBm), the exposure levels would be even lower.

B. OBU MEASUREMENTS

In this study, we measured the exposure levels inside and around an Audi A5 vehicle equipped with ITS-G5 technology, implemented through a Cohda MK5 OBU mounted on the vehicle. A 5.9 GHz antenna connected to the OBU was placed at two locations: near the front windshield and on the rear part of the vehicle roof. Fig. 13 summarizes
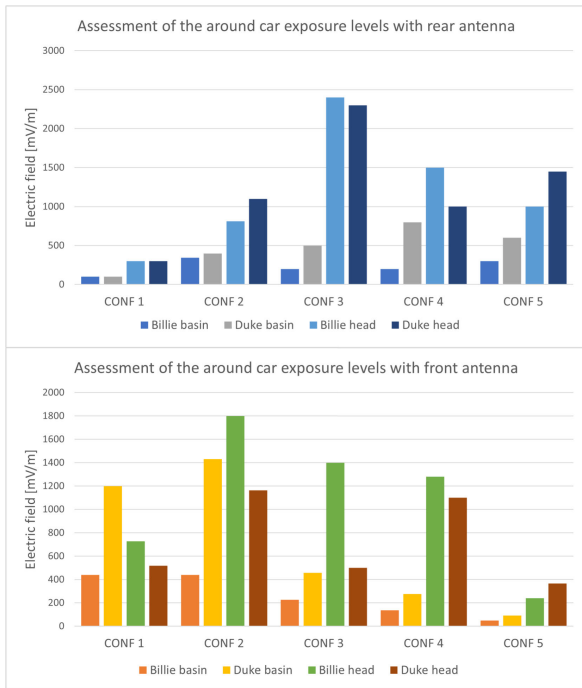
FIGURE 13. RMS values of the electric field E around the car (human beside) with antenna (input power of 33 dBm) positioned on the rear and front of the car roof.

FIGURE 14. Peak RMS values of the electric field E inside the car with antenna (input power of 33 dBm) positioned on the rear and front of the car roof.

the exposure levels at five positions around the vehicle at four different heights when the antenna was located at the front/rear roof positions, respectively. The highest exposure level occurred at position CONF 3 at the head height of the Billie model when the rear antenna switched on, measuring 2.4 V/m, which is only 4% of the ICNIRP reference level. When the front antenna was activated, the highest exposure level was found at position CONF 2, at the same height as the antenna installation, the head height of the Billie model (i.e., 1.36 m), measuring 1.8 V/m, which was the closest measurement point to the antenna. Compared to the rear antenna, higher exposure levels were often found at lower heights (Billie head or Duke basin) because the front antenna installation position is lower than the rear antenna, on the windscreen below the roof level. The shielding effect of the vehicle roof resulted in lower exposure levels at lower heights for the human model, i.e., the basin position, for the rear antenna.

Considering the worst-case scenario, with both front and rear antennas operating simultaneously, combining the two results yields the highest exposure measurement point still at the Billie head position at CONF 3, measuring 4.2 V/m or 6.9% of the ICNIRP limit. This result is similar to the RSU measurement results, where the highest exposure level was measured at the center position, equidistant from the two antennas, with the fields from both antennas superimposing to create a relatively larger field value at this position.

Fig. 14 compares the exposure levels at selected positions (head and basin) inside the vehicle at the five passenger
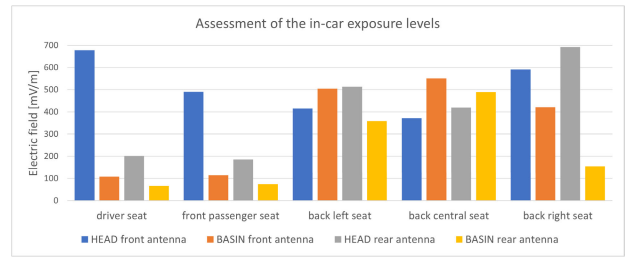
seats for both front and rear antennas. Compared to the measurements outside the car, the exposure level inside the car is substantially lower due to the shielding effect of the car body. In a comparison of the maximum values of electric field strength measured inside and outside the vehicle, the former is only one-third of the latter. It can be observed that in most scenarios, the head position always receives a higher exposure level, and the exposure levels at the head of rear passengers are similar for both front and rear antennas, making the head exposure level almost independent of the passenger's position. The maximum exposure was also found at the driver's seat head position when the front antenna was fed, measuring 0.68 V/m, and at the rear right passenger's head position when the rear antenna switched on, measuring 0.69 V/m, both less than 1.2% of the ICNIRP limit. It is also noted that for the basin position, exposure levels are lower in the front seats but relatively higher in the rear seats regardless of which antenna was operating, with the highest found in the back central seat at 0.55 V/m (0.9% of ICNIRP). Overall, back passengers receive higher electric field strength, especially considering the worst-case scenario, i.e., both front and rear antennas being excited simultaneously. The exposure levels at the heads of rear passengers could be twice that of front passengers and could reach up to six times at the basin position, yet still not exceeding 2% of the ICNIRP limit.

To facilitate comparison with our previous measurements of RSU exposure levels, when rescaling the RSU measurement results based on an antenna transmission power of 33 dBm, the maximum exposure level measured in close proximity to the RSU (at 0.5 m) was found to be 18.3 V/m. In real deployment scenarios for RSUs, the maximum exposure received by pedestrians and inside the vehicle was 256.8 mV/m and 39.2 mV/m, respectively. It is evident that, in scenarios close to the radiation source, humans could receive higher exposure levels from the RSU than from the OBU. However, such scenarios are more common in occupational exposures and are not prevalent in general public exposure settings. In real deployment cases for both RSU and OBU, the exposure levels generated by RSU to road users are significantly lower than those from the OBU, especially for exposure levels inside the vehicle, where RSU contributes only 6% (-25 dB) of that from

the OBU. Therefore, we can conclude that in novel V2X communication scenarios utilizing the ITS 5.9 GHz band, the RF EMF exposure to road users is predominantly contributed by OBUs.

Comparing recent studies, the placement of human models around the vehicle in the simulations by [19] is similar to the setup in this work. However, different from our findings, [19] found the highest SAR_{10g} in the head's skin tissue of human models at the rear of the vehicle, the position closest to the rear antenna. This discrepancy arises because, in our work, the CONF 5 position is not the closest to the rear antenna. Still, the location of maximum exposure in our study also is not the closest to the front/rear antennas. This reflects the complexity of 5.9 GHz field propagation in real-world scenarios, which is significantly influenced by the vehicle's size and the antenna's installation position. In [16], the exposure levels of Bluetooth, WiFi, and ITS-G5 technologies at nine different predefined points inside a vehicle were measured, with the ITS-G5 technology's two antennas located at the front windscreen and rear part of the roof, both with a maximum transmission power of 33 dBm. Reference [16] found that the antenna on the front windscreen of ITS-G5 produced the highest field at various points inside the vehicle, with the maximum exposure level found at the driver's seat trunk (defined as the basin in this study) being 3.3% of the ICNIRP reference level, significantly higher than the results measured at a similar position in this work (0.18% for the front antenna) and also higher than the maximum value found in this study (1.2%). This deviation could be because the front antenna in [16], a Di-patch antenna [15], might have a larger gain inside the vehicle, and the vehicle size also impacted the distribution of the field inside the car. Meanwhile, the exposure levels from the rear antenna in [16] were lower at all measured points inside the vehicle, not exceeding 0.2% of the ICNIRP reference level, which is less than the results found in this study. This is due to the installation position of the rear roof antenna in [16], which resulted in the vehicle body providing effective shielding for this antenna. It is also important to observe that variations in the measurement results are expected when considering different cars with different dimensions and shapes of windows and bodywork of the car.

C. TESLA MEASUREMENTS

Table. 3 summarizes the measurements of the maximum exposure levels E_{max} (RMS) from wireless RF technologies used by infotainment, sensing, and IoT devices on a vehicle. The average exposure levels E_{avg} were calculated based on the methodology described in [45]:

$$E_{avg} = \sqrt{DC} \cdot E_{max} \ (\text{V m}^{-1}). \tag{3}$$

Specifically, we evaluated the exposure levels of mmWave radar to pedestrians outside the vehicle, Bluetooth exposure levels at the driver and passenger positions inside the vehicle, and exposure from integrated LTE communication modules to pedestrians. Fig. 15 shows the spectrum of the mmWave
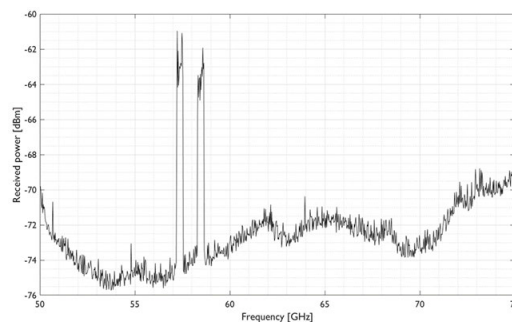

FIGURE 15. Frequency spectrum of the signal emitted by the mmWave radar at the headlight of Tesla Model S.

radar signal, revealing signal frequencies at 57.35 GHz and 58.45 GHz, both with a bandwidth of 300 MHz. Subsequently, we measured the signal amplitude and DC of the radar signal in the time domain using the zero-span mode of the SA. The maximum exposure level measured at a distance of 20 cm from the radar was 10.48 V/m, with the highest DC of 10%. Utilizing Equation (3), the average exposure level was calculated to be 3.31 V/m. Converting these values to power density in free space yields 0.29 W/m^2 and 0.029 W/m^2, respectively, for maximum and average exposure levels, both well below the ICNIRP limit of 10 W/m^2.

For the Bluetooth devices on the dashboard inside the vehicle, we found the highest exposure levels at the driver and passenger positions when the Bluetooth device was connected and communicating with a phone (playing Spotify), measuring 2.2 V/m (3.6% of the ICNIRP limit) and 1.2 V/m (2% of the ICNIRP), respectively, over twice the maximum values in other conditions and lower in the passenger's seat than in the driver's seat. However, it is important to note that in the Bluetooth connected case, the field is not solely from the vehicle's Bluetooth device but also from the Bluetooth antenna of the phone placed between the two seats. Bluetooth signals were detectable even when the Tesla was off, with signal strength and DC nearly at the same level as when the car was on and the Bluetooth device was idle. During the pairing search, although signal strength remained almost unchanged from the idle state, the DC was the highest at 7.8%, even exceeding that in the connected state, doubling the average exposure level from the idle state but still lower than in the connected state.

In this study, we measured the exposure levels at various distances from the integrated LTE module installed inside the vehicle's rearview mirror. Through broadband frequency-domain measurements, we observed the LTE1800 signal on the spectrum, including the uplink (UL) at 1720.3 MHz and the downlink (DL) at 1815.3 MHz. The maximum signal amplitude measured was 3.17 V/m (5.5% of the ICNIRP limit), with the probe in direct contact with the rearview mirror housing, i.e., 0 cm, then decreasing with distance. The DC of the LTE signal measured in various cases was

TABLE 3. Exposure and power levels for Tesla Model S wireless technologies, including mmWave radar, Bluetooth, and LTE modules, are provided. E_{max} is the peak electric field (RMS), DC is the duty cycle, and E_{avg} is the average exposure calculated from DC and E_{max}.

Source	Measurement setups	E_{max} (V/m)	DC (%)	E_{avg} (V/m)	Power level (dBm)
Radar	Probe above headlight				55
	20 cm	10.48	10	3.31	
Bluetooth	Probe in driver's seat				20
	Tesla Off	1.29	1.0	0.13	
	Idle	1.09	1.5	0.13	
	Searching	1.01	7.8	0.28	
	Connected (phone between seats)	2.22	5.3	0.51	
	Probe in passenger's seat				
	Tesla Off	0.57	1.7	0.08	
	Idle	0.45	1.3	0.05	
	Searching	0.56	7.8	0.16	
	Connected (phone between seats)	1.18	5.4	0.26	
Integrated LTE connection	Next to the right rearview mirror				23
	0 cm				
	Tesla Off	1.93	5.2	0.44	
	Tesla On	3.17	8.2	0.91	
	15 cm				
	Tesla Off	2.98	7.0	0.79	
	Tesla On	2.93	5.9	0.71	
	50 cm				
	Tesla Off	1.68	4.3	0.35	
	Tesla On	1.75	7.7	0.49	

between 5-8%, yielding a maximum average exposure level of 0.91 V/m (1.5% of the ICNIRP limit), only a third of the maximum exposure level. Similar to in-vehicle Bluetooth devices integrated LTE modules continue to transmit signals with unchanged amplitude and DC when the vehicle is off. So pedestrians around the vehicle or passengers inside could potentially be exposed to the RF EMF from these devices.

In [27], the authors measured the spatial average power density of the vehicle's 60 GHz mmWave radar, finding around 5 W/m² at 30 mm from the radar, significantly higher than 0.29 W/m² measured 20 cm from the front lights in this study, possibly due to the larger path loss at mmWave frequencies. This difference is also due to [27] setting the radar to transmit with an input power of 10 dBm with a 100% DC for worst-case scenarios, whereas the actual maximum transmission power of the radar is considered here. Reference [52] measured the electric field distribution inside a vehicle with a case of the phone turned off and another case which is during a Bluetooth-connected call. The maximum exposure level found at a measurement point above the driver's seat for the 2.4 GHz-2.8 GHz frequency band used by Bluetooth technology was 218.1 mV/m, corresponding to the Bluetooth call case. This result is not on the same order of magnitude as the highest field strength found in this study, likely due to differences in the devices' maximum transmission power among manufacturers, the considered configurations, and devices not necessarily operating at maximum transmission power in real scenarios, thus only a qualitative comparison is made with [52]'s results. Similar to our findings, [52] found that switching from off (i.e., the

idle state in our study) to Bluetooth calling, the exposure level nearly tripled. Reference [16]'s maximum measurement of the field produced by Bluetooth technology at the driver's trunk was 0.61 V/m, lower than our findings at the driver's position and similar to our measurements at the passenger's position. It is important to note we do not know the operating state of the in-vehicle Bluetooth device during [16]'s measurements.

D. CUMULATIVE EXPOSURE LEVELS
Our study has found that individual devices —whether they be RSU communication modules, OBU systems, or Tesla's onboard technologies —consistently operate below the ICNIRP reference levels for general public exposure. However, the real-world scenario often involves the simultaneous functioning of multiple devices which could potentially amplify the cumulative exposure. Therefore, it is necessary to assess the cumulative exposure levels of road users in V2X scenarios, across various technology frequencies, based on our experimental measurements. To facilitate the assessment of this cumulative exposure, we have defined a cumulative exposure index I_{cum}, in accordance with ICNIRP guidelines [42]:

$$I_{cum} = \sum_{i>30\,\text{MHz}}^{2\,\text{GHz}} \left(\frac{E_{max,i}}{E_{RL,i}}\right)^2 + \sum_{i>2\,\text{GHz}}^{300\,\text{GHz}} \left(\frac{S_{max,i}}{S_{RL,i}}\right) \quad (4)$$

where, $E_{max,i}$ and $S_{max,i}$ represent the maximum measured electric field strength and power density, respectively, while $E_{RL,i}$ and $S_{RL,i}$ are ICNIRP's reference levels for public
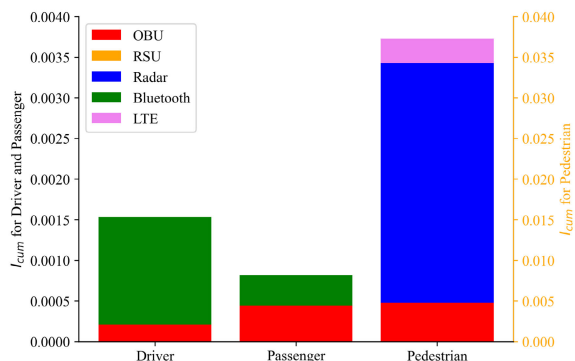
FIGURE 16. Cumulative exposure indices for drivers, passengers, and pedestrians for each wireless technology, where RSU data are used from in-situ measurements.

TABLE 4. The maximum exposure levels found across all measurements in this study, and their comparison to ICNIRP limits.

Exposure scenarios	Frequency	Max exposure	dB of ICNIRP reference level
V2X-RSU	5.9 GHz		
in-lab		0.089 W/m^2	-20.5
in-situ		0.017 mW/m^2	-57.7
V2X-OBU	5.9 GHz		
around car		0.015 W/m^2	-28.2
in-car		1.26 mW/m^2	-39.0
Bluetooth integrated inside the car	2.4 GHz	0.013 W/m^2	-28.9
LTE1800 integrated on the car	1.8 GHz	3.17 V/m	-25.2
ADAS radar on the car	60 GHz	0.29 W/m^2	-15.4

Following ICNIRP guidelines, for those frequencies>2 GHz to 300 GHz: the measured electric field strengths are converted to EMF power densities using the Equation (1).

exposure to electric field strength and power density, and i indicates the corresponding frequency.

It is evident that higher exposure levels across frequencies result in a higher cumulative I_{cum}. A value of I_{cum} exceeding 1 indicates that the cumulative exposure level surpasses ICNIRP guidelines. In this study, we evaluated the cumulative exposure levels experienced by drivers and passengers inside vehicles, as well as pedestrians outside the vehicle, considering the worst-case scenario, i.e., using the maximum exposure levels measured for each technology (for RSU, the results from in-situ measurements were used) inside and outside the vehicle. Although such exposure scenarios are unlikely in real environments, this study only involves a single connected vehicle. In real traffic scenarios, such as on congested main roads, road users would be exposed to radiation from multiple vehicles/infrastructure communication technologies simultaneously. Therefore, calculating the cumulative exposure level for the worst-case scenario to estimate the upper limit of exposure in a single-vehicle scenario is meaningful.

Fig. 16 presents the cumulative exposure indices I_{cum} for drivers, passengers inside vehicles, and pedestrians outside, as calculated from our measurements. The maximum value observed was merely 0.037, substantially below the ICNIRP guidelines. The contribution of RSU, deployed at gantries in real-world scenarios, to the overall cumulative exposure, is negligible. In contrast, pedestrians around vehicles may experience higher cumulative exposures due to the externally installed communication technologies e.g., LTE and ITS-G5, which are designed for longer-range communications and feature higher antenna gains and transmission power. Furthermore, the mmWave radar around 60 GHz contributes 79% to the pedestrian cumulative exposure index due to its high frequency and power. Inside the vehicle, radiation sources primarily originate from infotainment devices utilizing Bluetooth technology, which is intended for short-range communication with a lower transmission power (0.1 W). Additionally, the metallic body of the vehicle provides electromagnetic shielding, resulting in lower exposure levels from the OBU for occupants inside the vehicle compared to pedestrians, hence the very low cumulative exposure levels for vehicle occupants.

Our analysis highlights the significant role that mmWave radars play in the cumulative electromagnetic exposure within the smart connected car ecosystem. However, this study did not assess the electric field strength produced inside adjacent vehicle cabins by the mmWave radars. The study by Ruddle [23] employed the power balance method to estimate the electric field strength at frequencies of 24/46.8/77 GHz, coupling through car windows into the vehicle interior. In a worst-case scenario, where a vehicle is irradiated by radars on all four sides (i.e., front and rear, left and right), at the frequency of 77 GHz with an EIRP of 50 dBm, the coupled power density inside the vehicle was found to be 3.55 W/m^2. Considering all different frequency radiation sources both inside and outside the vehicle (e.g., 0.9-2.1 GHz mobile phones, 2.4 GHz Bluetooth, 5.8 GHz toll beacons), the 77 GHz radars contributed 44.5% to the total cumulative exposure inside the vehicle. Although the [23]'s assumption of uniformly distributed and normal incidence of external sources at the car windows may overestimate the exposure levels, the prominent role of mmWave radars in exposure assessments both inside and outside vehicles is evident.

Importantly, the advent of 5G/6G technologies for V2X communications will prominently feature the mmWave bands, such as the 5G NR's FR2 band range from 24.25 to 52.6 GHz. Moreover, the integration of Multiple-Input Multiple-Output (MIMO) antennas for these innovation technologies, which employ sophisticated beamforming techniques, poses new challenges for the assessment of EMF exposure. These antennas' ability to direct power more precisely may alter exposure patterns, necessitating refined measurement and modeling techniques to quantify EMF in dense traffic environments accurately. Future studies should therefore focus on developing new methodologies for reliably

assessing the EMF exposure contributed by these advanced communication technologies. The integration and cumulative effects of multiple sources of radiation in the V2X ecosystem should also be considered.

IV. CONCLUSION

This study proposes a comprehensive assessment of RF exposure from ITS-5.9 GHz V2X technologies, including RSUs, OBUs, and integrated systems in a Tesla Model S including DC and power levels. Our combined approach of numerical dosimetry and experimental measurements confirms that RF exposure levels are well below ICNIRP guidelines across all scenarios investigated, with the highest local SAR_{10g} and WBS at 5.9 GHz not exceeding -8 dB and -18 dB, respectively, of the limits specified by ICNIRP. Table. 4 summarizes the maximum exposure levels found across all measurements of this study, compared against the ICNIRP reference levels (in terms of dB of ICNIRP limits). The exposure from Tesla is predominated by its mmWave radar, which is well within safe limits, underscoring the safety of these technologies. These findings validate the effectiveness of current V2X communication systems and support their safe integration into intelligent transportation systems. Future work will consist of exposure assessment from forthcoming 5G and 6G technologies for connected car mobility.

REFERENCES

[1] G. Tognola, B. Masini, S. Gallucci, M. Bonato, S. Fiocchi, E. Chiaramello, M. Parazzini, and P. Ravazzani, "Numerical assessment of RF human exposure in smart mobility communications," *IEEE J. Electromagn., RF Microw. Med. Biol.*, vol. 5, no. 2, pp. 100–107, Jun. 2021. [Online]. Available: https://ieeexplore.ieee.org/document/9142353/

[2] K. Sjoberg, P. Andres, T. Buburuzan, and A. Brakemeier, "Cooperative intelligent transport systems in europe: Current deployment status and outlook," *IEEE Veh. Technol. Mag.*, vol. 12, no. 2, pp. 89–97, Jun. 2017.

[3] S.-W. Leung, Y. Diao, K.-H. Chan, Y.-M. Siu, and Y. Wu, "Specific absorption rate evaluation for passengers using wireless communication devices inside vehicles with different handedness, passenger counts, and seating locations," *IEEE Trans. Biomed. Eng.*, vol. 59, no. 10, pp. 2905–2912, Oct. 2012. [Online]. Available: http://ieeexplore.ieee.org/document/6263283/

[4] L.-R. Harris, M. Zhadobov, N. Chahat, and R. Sauleau, "Electromagnetic dosimetry for adult and child models within a car: Multi-exposure scenarios," *Int. J. Microw. Wireless Technol.*, vol. 3, no. 6, pp. 707–715, Dec. 2011.

[5] E. Aguirre, P. L. Iturri, L. Azpilicueta, S. de Miguel-Bilbao, V. Ramos, U. Gárate, and F. Falcone, "Analysis of estimation of electromagnetic dosimetric values from non-ionizing radiofrequency fields in conventional road vehicle environments," *Electromagn. Biol. Med.*, vol. 34, no. 1, pp. 19–28, Jan. 2015. [Online]. Available: http://www.tandfonline.com/doi/full/10.3109/15368378.2013.863782

[6] M. Celaya-Echarri, L. Azpilicueta, P. Lopez-Iturri, E. Aguirre, S. De Miguel-Bilbao, V. Ramos, and F. Falcone, "Spatial characterization of personal RF-EMF exposure in public transportation buses," *IEEE Access*, vol. 7, pp. 33038–33054, 2019. [Online]. Available: https://ieeexplore.ieee.org/document/8662564/

[7] Z. Judakova and L. Janousek, "Possible health impacts of advanced vehicles wireless technologies," *Transp. Res. Proc.*, vol. 40, pp. 1404–1411, 2019. [Online]. Available: https://linkinghub.elsevier.com/retrieve/pii/S2352146519303643

[8] M. Eeftens, B. Struchen, L. E. Birks, E. Cardis, M. Estarlich, M. F. Fernandez, P. Gajšek, M. Gallastegi, A. Huss, L. Kheifets, I. K. Meder, J. Olsen, M. Torrent, T. Trcek, B. Valic, R. Vermeulen, M. Vrijheid, L. van Wel, M. Guxens, and M. Röösli, "Personal exposure to radio-frequency electromagnetic fields in Europe: Is there a generation gap?" *Environ. Int.*, vol. 121, pp. 216–226, Dec. 2018. [Online]. Available: https://linkinghub.elsevier.com/retrieve/pii/S0160412018306962

[9] S. Sagar, S. M. Adem, B. Struchen, S. P. Loughran, M. E. Brunjes, L. Arangua, M. A. Dalvie, R. J. Croft, M. Jerrett, J. M. Moskowitz, T. Kuo, and M. Röösli, "Comparison of radiofrequency electromagnetic field exposure levels in different everyday microenvironments in an international context," *Environ. Int.*, vol. 114, pp. 297–306, May 2018. [Online]. Available: https://linkinghub.elsevier.com/retrieve/pii/S016041201731485X

[10] K. Roser, A. Schoeni, B. Struchen, M. Zahner, M. Eeftens, J. Fröhlich, and M. Röösli, "Personal radiofrequency electromagnetic field exposure measurements in Swiss adolescents," *Environ. Int.*, vol. 99, pp. 303–314, Feb. 2017. [Online]. Available: https://linkinghub.elsevier.com/retrieve/pii/S016041201630527X

[11] G. Tognola, M. Bonato, M. Benini, S. Aerts, S. Gallucci, E. Chiaramello, S. Fiocchi, M. Parazzini, B. M. Masini, W. Joseph, J. Wiart, and P. Ravazzani, "Survey of exposure to RF electromagnetic fields in the connected car," *IEEE Access*, vol. 10, pp. 47764–47781, 2022.

[12] D. Kornek, M. Schack, E. Slottke, O. Klemp, I. Rolfes, and T. Kürner, "Effects of antenna characteristics and placements on a vehicle-to-vehicle channel scenario," in *Proc. IEEE Int. Conf. Commun. Workshops*. Cape Town, South Africa: IEEE, May 2010, pp. 1–5. [Online]. Available: http://ieeexplore.ieee.org/document/5503935/

[13] E. Whalen, A. Elfrgani, C. Reddy, and R. Rajan, "Antenna placement optimization for vehicle-to-vehicle communications," in *Proc. IEEE Int. Symp. Antennas Propag. USNC/URSI Nat. Radio Sci. Meeting*, Boston, MA, USA, Jul. 2018, pp. 1673–1674. [Online]. Available: https://ieeexplore.ieee.org/document/8609047/

[14] G. Artner, W. Kotterman, G. Del Galdo, and M. A. Hein, "Automotive antenna roof for cooperative connected driving," *IEEE Access*, vol. 7, pp. 20083–20090, 2019. [Online]. Available: https://ieeexplore.ieee.org/document/8633835/

[15] J. Singh, R. Stephan, and M. A. Hein, "Low-profile wideband differentially fed di-patch antenna closely above metallic ground," *IEEE Antennas Wireless Propag. Lett.*, vol. 18, pp. 976–980, 2019. [Online]. Available: https://ieeexplore.ieee.org/document/8675408/

[16] L.-M. Schilling, C. Bornkessel, and M. A. Hein, "Human RF electromagnetic exposure to V2X-communication," *Adv. Radio Sci.*, vol. 19, pp. 233–239, Sep. 2022. [Online]. Available: https://ars.copernicus.org/articles/19/233/2022/

[17] M. Bonato, G. Tognola, M. Benini, S. Gallucci, E. Chiaramello, S. Fiocchi, and M. Parazzini, "Assessment of SAR in road-users from 5G-V2X vehicular connectivity based on computational simulations," *Sensors*, vol. 22, no. 17, p. 6564, Aug. 2022. [Online]. Available: https://www.mdpi.com/1424-8220/22/17/6564

[18] M. Bonato, G. Tognola, M. Benini, S. Gallucci, E. Chiaramello, S. Fiocchi, and M. Parazzini, "Stochastic dosimetry assessment of human RF-EMF spatial exposure variability in 5G-V2X vehicular communication scenario," *IEEE Access*, vol. 11, pp. 94962–94973, 2023. [Online]. Available: https://ieeexplore.ieee.org/document/10235974/

[19] M. Benini, M. Parazzini, M. Bonato, S. Gallucci, E. Chiaramello, S. Fiocchi, and G. Tognola, "Road user exposure from ITS-5.9 GHz vehicular connectivity," *Sensors*, vol. 22, no. 18, p. 6986, Sep. 2022. [Online]. Available: https://www.mdpi.com/1424-8220/22/18/6986

[20] M. Benini, M. Parazzini, M. Bonato, S. Gallucci, E. Chiaramello, S. Fiocchi, and G. Tognola, "Assessment of children's exposure to intelligent transport system 5.9 GHz vehicular connectivity using numerical dosimetry," *Sensors*, vol. 23, no. 11, p. 5170, May 2023. [Online]. Available: https://www.mdpi.com/1424-8220/23/11/5170

[21] M. Benini, S. Gallucci, M. Bonato, M. Parazzini, and G. Tognola, "Evaluation of road user radio-frequency exposure levels in an urban environment from vehicular antennas and the infrastructure in ITS-G5 5.9 GHz communication," *IEEE Access*, vol. 12, pp. 51419–51430, 2024.

[22] G. Tognola, M. Benini, M. Bonato, S. Gallucci, and M. Parazzini, "Assessment of the variability of human exposure to radiofrequency electromagnetic fields arising from 5.9 GHz vehicular communication in urban environments," *Sensors*, vol. 23, no. 15, p. 6802, Jul. 2023. [Online]. Available: https://www.mdpi.com/1424-8220/23/15/6802

[23] A. R. Ruddle, "Preliminary estimates of electromagnetic field exposures due to advanced vehicle technologies," in *Proc. Loughborough Antennas Propag. Conf. (LAPC)*, Loughborough, Leicestershire, U.K., Nov. 2016, pp. 1–5. [Online]. Available: http://ieeexplore.ieee.org/document/7807587/

[24] Z. Vilagosh, A. Lajevardipour, and A. Wood, "Computer simulation study of the penetration of pulsed 30, 60 and 90 GHz radiation into the human ear," *Sci. Rep.*, vol. 10, no. 1, p. 1479, Jan. 2020. [Online]. Available: https://www.nature.com/articles/s41598-020-58091-7

[25] I. Laakso, R. Morimoto, J. Heinonen, K. Jokela, and A. Hirata, "Human exposure to pulsed fields in the frequency range from 6 to 100 GHz," *Phys. Med. Biol.*, vol. 62, no. 17, pp. 6980–6992, Aug. 2017. [Online]. Available: https://iopscience.iop.org/article/10.1088/1361-6560/aa81fe

[26] N. Simicevic, "Dosimetric implication of exposure of human eye to ultra-wideband electromagnetic pulses," in *Proc. Asia–Pacific Symp. Electromagn. Compat. 19th Int. Zurich Symp. Electromagn. Compat.*, Singapore, May 2008, pp. 208–211. [Online]. Available: http://ieeexplore.ieee.org/document/4559848/

[27] G. Vermeeren, S. Kühn, B. Debaillie, G. Torfs, N. Kuster, P. Demeester, W. V. Thillo, L. Martens, and W. Joseph, "Exposure assessment of 60 GHz communication antenna and 79 GHz automotive radar," in *Proc. Joint Annu. Meeting Bioelectromagnetics Soc. Eur. BioElectromagnetics Assoc.*, 2018.

[28] *MK5 RSU—Cohda Wireless*. [Online]. Available: https://www.cohdawireless.com/solutions/hardware/mk5-rsu/

[29] *IEEE Standard for Information Technology–Telecommunications and Information Exchange Between Systems–Local and Metropolitan Area Networks–Specific Requirements Part 11: Wireless LAN Medium Access Control (MAC) and Physical Layer (PHY) Specifications Amendment 6: Wireless Access in Vehicular Environments*, 2010.

[30] *Intelligent Transport Systems (ITS); Radiocommunications Equipment Operating in the 5855 MHz to 5925 MHz Frequency Band; Harmonised Standard Covering the Essential Requirements of Article 3.2 of Directive 2014/53/EU*, 2017.

[31] *MK6C EVK*. [Online]. Available: https://www.cohdawireless.com/solutions/hardware/mk6c-evk/

[32] *Intelligent Transport Systems (ITS); LTE-V2X Access Layer Specification for Intelligent Transport Systems Operating in the 5 GHz Frequency Band*, Standard ETSI EN 303 613, Jan. 10, 2021.

[33] *LTE; Evolved Universal Terrestrial Radio Access (E-UTRA); User Equipment (UE) Radio Transmission and Reception (3GPP TS 36.101 version 14.20.0 Release 14)*, 2021.

[34] *3rd Generation Partnership Project; Technical Specification Group Radio Access Network; Study on LTE-Based V2X Services; (Release 14)*, 2016.

[35] *USRP N310 | Ettus Research, a National Instruments Brand | The Leader in Software Defined Radio (SDR)*. [Online]. Available: https://www.ettus.com/all-products/usrp-n310/

[36] *Technical Specification Group Radio Access Network; V2X Services Based on NR; User Equipment (UE) Radio Transmission and Reception; (Release 16)*, 2021.

[37] *Technical Specification Group Radio Access Network; NR Sidelink Enhancement; User Equipment (UE) Radio Transmission and Reception; (Release 17)*, 2022.

[38] M.-C. Gosselin, E. Neufeld, H. Moser, E. Huber, S. Farcito, L. Gerber, M. Jedensjö, I. Hilber, F. D. Gennaro, B. Lloyd, E. Cherubini, D. Szczerba, W. Kainz, and N. Kuster, "Development of a new generation of high-resolution anatomical models for medical device evaluation: The virtual population 3.0," *Phys. Med. Biol.*, vol. 59, no. 18, pp. 5287–5303, Sep. 2014. [Online]. Available: https://iopscience.iop.org/article/10.1088/0031-9155/59/18/5287

[39] A. Christ, W. Kainz, E. G. Hahn, K. Honegger, M. Zefferer, E. Neufeld, W. Rascher, R. Janka, W. Bautz, J. Chen, B. Kiefer, P. Schmitt, H.-P. Hollenbach, J. Shen, M. Oberle, D. Szczerba, A. Kam, J. W. Guag, and N. Kuster, "The virtual family—Development of surface-based anatomical models of two adults and two children for dosimetric simulations," *Phys. Med. Biol.*, vol. 55, no. 2, pp. N23–N38, Jan. 2010. [Online]. Available: https://iopscience.iop.org/article/10.1088/0031-9155/55/2/N01

[40] *Sim4life*. [Online]. Available: https://sim4life.swiss/

[41] S. Gabriel, R. W. Lau, and C. Gabriel, "The dielectric properties of biological tissues: II. Measurements in the frequency range 10 Hz to 20 GHz," *Phys. Med. Biol.*, vol. 41, no. 11, pp. 2251–2269, Nov. 1996. [Online]. Available: https://iopscience.iop.org/article/10.1088/0031-9155/41/11/002

[42] "Guidelines for Limiting Exposure to Electromagnetic Fields (100 kHz to 300 GHz)," *Health Phys.*, vol. 118, no. 5, pp. 483–524, May 2020. [Online]. Available: https://journals.lww.com/10.1097/HP.0000000000001210

[43] J. Marquez-Barja, B. Lannoo, D. Naudts, B. Braem, C. Donato, V. Maglogiannis, S. Mercelis, R. Berkvens, P. Hellinckx, M. Weyn, I. Moerman, and S. Latre, "Smart highway: Its-G5 and C-V2X based testbed for vehicular communications in real environments enhanced by edge/cloud technologies," in *Proc. Eur. Conf. Netw. Commun.*, 2019.

[44] L. Verloock, W. Joseph, G. Vermeeren, and L. Martens, "Procedure for assessment of general public exposure from WLAN in offices and in wireless sensor network testbed," *Health Phys.*, vol. 98, no. 4, pp. 628–638, Apr. 2010.

[45] W. Joseph, D. Pareit, G. Vermeeren, D. Naudts, L. Verloock, L. Martens, and I. Moerman, "Determination of the duty cycle of WLAN for realistic radio frequency electromagnetic field exposure assessment," *Prog. Biophys. Mol. Biol.*, vol. 111, no. 1, pp. 30–36, Jan. 2013. [Online]. Available: https://linkinghub.elsevier.com/retrieve/pii/S0079610712001083

[46] S. Aerts, L. Verloock, M. Van den Bossche, L. Martens, X. Vergara, and W. Joseph, "Emissions from smart meters and other residential radiofrequency sources," *Health Phys.*, vol. 116, no. 6, pp. 776–788, Jun. 2019. [Online]. Available: https://journals.lww.com/00004032-201906000-00004

[47] S. Aerts, M. Van den Bossche, X. Vergara, S. Odie, L. Verloock, L. Martens, and W. Joseph, "Spatial and temporal assessment of radiofrequency electromagnetic fields emitted by smart meters and smart meter banks in urban environments," *Environ. Res.*, vol. 183, Apr. 2020, Art. no. 109196. [Online]. Available: https://linkinghub.elsevier.com/retrieve/pii/S0013935120300888

[48] *V-Band, Wr-15, Omnidirectional Antenna*. [Online]. Available: https://www.miwv.com/v-band-wr-15-omnidirectional-antenna/

[49] L. Low, A. R. Ruddle, J. M. Rigelsford, and R. J. Langley, "Computed impact of human occupants on field distributions within a passenger vehicle," in *Proc. 6th Eur. Conf. Antennas Propag. (EUCAP)*. Prague, Czech Republic: IEEE, Mar. 2012, pp. 1214–1217. [Online]. Available: http://ieeexplore.ieee.org/document/6205898/

[50] *IEC/IEEE International Standard—Determining the peak Spatial-Average Specific Absorption Rate (SAR) in the Human Body From Wireless Communications Devices, 30 MHz to 6 GHz—Part 1: General Requirements for Using the Finite-Difference Time-Domain (FDTD) Method for SAR Calculations*.

[51] (2019). *IEEE Standard for Safety Levels With Respect To Human Exposure To Electric, Magnetic, and Electromagnetic Fields, 0 Hz To 300 GHz*. [Online]. Available: https://ieeexplore.ieee.org/document/8859679/

[52] Z. Psenakova, D. Gombárska, and M. Smetana, "Electromagnetic field measurement inside the car with modern embedded wireless technologies," in *Proc. IEEE 21st Int. Conf. Comput. Problems Electr. Eng. (CPEE)*. Poland: IEEE, Sep. 2020, pp. 1–4. [Online]. Available: https://ieeexplore.ieee.org/document/9238731/

YIZHEN YANG received the dual B.S. degree in electronics and information from Xidian University, Xi'an, China, and Sorbonne University, Paris, France, in 2018, and the M.S. degree in electrical engineering from Sorbonne University, in 2020. He is currently pursuing the Ph.D. degree with the WAVES Research Group, Ghent University/imec, Ghent, Belgium. He was involved in the research and development of RF phased array coils for clinical magnetic resonance imaging (MRI) systems within the industry, from 2020 to 2022. His research interests include RF-EMF exposure, biomedical in/on-body antennas, in-to-on-body EMF propagation, and micro-dosimetry.

BARBARA M. MASINI (Senior Member, IEEE) received the Laurea degree (summa cum laude) and the Ph.D. degree in telecommunications engineering from the University of Bologna, Italy, in 2001 and 2005, respectively. She is currently a Senior Researcher with the Institute of Electronics, Computer and Telecommunication Engineering, National Research Council (CNR), Italy. She is also an Adjunct Professor with the University of Bologna and an Associate Member of CNIT/Wilab, Italy. She works in the area of wireless communication systems and her research interests include connected vehicles, from physical and MAC levels aspects up to applications and field trial implementations. She is responsible for a number of national and international projects on vehicular communications and urban intelligence and responsible for the design and test of field trials on cooperative connected vehicles. Her research is also focused on relay-assisted communications, energy harvesting, and visible light communication. She is an Editor of IEEE Access and *Computer Communication* (Elsevier).

GÜNTER VERMEEREN (Member, IEEE) received the M.Sc. degree in industrial engineering from KAHO Sint-Lieven, Ghent, Belgium, in July 1998, and the M.Sc. degree in electrical engineering and the Ph.D. degree in electrotechnical engineering from Ghent University, Ghent, in July 2001 and August 2013, respectively. From September 2001 to September 2002, he was with the Research and Development Department, Network Integrator Telindus, Leuven, Belgium. Since September 2002, he has been a Research Engineer with the WiCa Group, Department of Information Technology, Ghent University. His research interests include numerical modeling and measurements of electromagnetic radiation in the domain of radio frequency dosimetry, electromagnetic exposure, on-body propagation, interference in communication networks, and medical imaging systems, such as hybrid magnetic resonance imaging (MRI) systems.

DANIEL VAN DEN AKKER received the master's degree in computer science from the University of Antwerp, in June 2009, and the Ph.D. degree in computer sciences, in September 2020. After obtaining an Aspirant Grant from the Fund for Scientific Research Flanders (FWO), he joined the "Internet and Data Laboratory" Research Group, in October 2009. Since then, he has been working on diverse research projects involving wireless communication. His work initially focused on sensor networks and smart cities. More recently, he has been involved in research projects about V2X and 5G communication. He currently manages the smart highway and Citylab testbeds located in Antwerp.

SAM AERTS was born in Sint-Niklaas, Belgium, in 1988. He received the M.Sc. degree in applied physics and the Ph.D. degree in electrical engineering from Ghent University (UGent), Ghent, Belgium, in 2011 and 2017, respectively. Since 2017, he has been a Postdoctoral Fellow with the Research Foundation—Flanders (FWO), Belgium, and the WAVES Research Group, IMEC, UGent.

LEEN VERLOOCK was born in Eeklo, Belgium, in November 1979. She received the master's degree in electronics engineering from Katholieke Hogeschool Ghent, Ghent, Belgium, in 2001. From September 2001 to September 2005, she was with the IMEC, Department of Information Technology (INTEC), Ghent University, where she was a Technical and Research Assistant with the Wireless and Cable Research Group. Since October 2005, she has been with the Wireless and Cable Research Group, Ghent University, and continues her work as before. She is working on propagation effects for wireless systems, including the influence of the user on this propagation, and on measurement procedures to assess electromagnetic field exposure of new wireless technologies, such as LTE, and 5G NR. Furthermore, she is responsible for the in-situ electromagnetic field measurements (by order of the government, telecommunication operators, and companies) for compliance evaluation with regional and international guidelines. She also assists Ph.D. students with their research on modeling and measuring the propagating fields of wireless systems.

EMMA CHIARAMELLO (Member, IEEE) received the master's and Ph.D. degrees in biomedical engineering from Politecnico di Torino, Turin, Italy, in 2009 and 2013, respectively. She is currently a Research Scientist with the Institute of Electronics, Computer, and Telecommunication Engineering, National Research Council of Italy, Rome, Italy. Her research interests include the study of the interactions between EMF and biological systems, with both deterministic dosimetry based on computational electromagnetism methods and stochastic dosimetry based on surrogate modeling.

MARTA BONATO received the master's and Ph.D. degrees in biomedical engineering from the Polytechnic University of Milan, Milan, Italy, in 2017 and 2021, respectively. She is currently a Research Scientist with the Institute of Electronics, Computer, and Telecommunication Engineering, National Research Council of Italy, Rome, Italy. Her research interests include the study of the interaction of electromagnetic fields (EMF) with biological systems and the study of possible effects of EMF on health with both deterministic and stochastic dosimetry, particularly from 5G networks.

JOE WIART (Senior Member, IEEE) received the Ph.D. degree, in 1995, and the H.D.R. degree, in 2015. He was an Ingenieur General des Mines. Since 2015, he has been the Chair C2M "Characterization, Modeling and Master of the Institut Mines-Télécom," Télécom Paris, Institut Polytechnique de Paris. He is also the Chairperson of the TC106x of the CENELEC in-charge of EMF exposure standards. He has been the Chair of URSI Commission K (electromagnetic fields and biological systems), from 2014 to 2021. His works gave rise to more than 150 publications in journal articles and more than 200 communications. His research interests include experimental, numerical methods, machine learning, artificial intelligence, and statistics applied in electromagnetism and dosimetry.

WOUT JOSEPH (Senior Member, IEEE) was born in Ostend, Belgium, in October 1977. He received the M.Sc. degree in electrical engineering from Ghent University, Belgium, in July 2000, and the Ph.D. degree, in March 2005. His Ph.D. work dealt with measuring and modeling of electromagnetic fields around base stations for mobile communications related to the health effects of exposure to electromagnetic radiation. From 2007 to 2012, he was a Postdoctoral Fellow of the Research Foundation—Flanders (FWO-V). Since October 2009, he has been a Professor in the domain of experimental characterization of wireless communication systems. He has been an imec PI, since 2017. His research interests include electromagnetic field exposure assessment, propagation for wireless communication systems, antennas, and calibration. He specializes in wireless performance analysis and quality of experience.

● ● ●

GABRIELLA TOGNOLA received the master's degree in electronic engineering and the Ph.D. degree in bioengineering from Politecnico di Milano, Milan, Italy. She is currently the Director of Research with the Institute of Electronics, Computer and Telecommunication Engineering, Consiglio Nazionale delle Ricerche. Her main research interests include exposure assessment of electromagnetic fields with numerical dosimetry and with machine learning methods and modeling of electromagnetic fields for biomedical applications and innovative EMF applications in connected vehicles.